DIVALENT ION-BINDING AND THERMAL STABILITY STUDIES ON RAT β-PARVALBUMIN AND THE EVIDENCE OF INFLUENTIAL DISTANT AMINO ACID RESIDUES AFFECTING CD SITE ION AFFINITY

A Thesis presented to the Faculty of the Graduate School

University of Missouri-Columbia

In Partial Fulfillment of the

Requirements for the Degree Master of Science

---

by

KELLY NDUBUKA

Dr. Michael T. Henzl, Thesis Supervisor

MAY 2011

The undersigned, appointed by the Dean of the Graduate School, have examined the thesis entitled

DIVALENT ION-BINDING AND THERMAL STABILITY STUDIES ON RAT β-PARVALBUMIN AND THE EVIDENCE OF INFLUENTIAL DISTANT AMINO ACID RESIDUES AFFECTING CD SITE ION AFFINITY

Presented by Kelly Ndubuka

a candidate for the degree of Master of Science,

and hereby certify that, in their opinion, it is worthy of acceptance.

Dr. Michael T. Henzl

Dr. Charlotte L. Phillips

Dr. John J. Tanner

I would like to thank everybody who made this possible. Special mention goes to my family; The Royal Momsie Chinyere I. Ndubuka, Chinwe “Ticho” Ndubuka, Mickey “Swaye” Ndubuka, Eze “Nigorian” Ndubuka, Chiamaka “Jameck” Ndubuka and The Royal Popsie himself, Dr. Bennett Ndubuka.

ACKNOWLEDGEMENTS

I hereby wish to acknowledge the invaluable guidance and instruction from Dr. Michael T. Henzl over the years that ultimately afforded me the opportunity of realizing this goal. It is very well appreciated.

TABLE OF CONTENTS

LIST OF TABLES

LIST OF FIGURES

ABBREVIATIONS

ATH, avian thymic hormone

CPV3, chicken parvalbumin 3

DARPP, dopamine- and cyclic AMP-regulated phosphoprotein

DEAE-Sepharose, diethylaminoethyl Sepharose

DMPC, dimyristoylphosphatidylcholine

DPPC, dipalmitoyl Phosphatidylcholine

DSC, differential scanning calorimetry

DSPC, distearoylphosphatidylcholine

DTT, dithiothreitol

EDTA, ethylenediamine tetraacetic acid

HEPES, 4-(2-hydroxyethyl 1)-1-piperazineethanesulfonic acid

HLH, helix-loop-helix

ITC, isothermal titration calorimetry

LB, Luria-Bertani growth medium

LB/amp, Luria-Bertani growth medium/ampicillin

OM, oncomodulin (rat β–parvalbumin)

NTA, nitrilotriacetic acid

PAGE, polyacrylamide gel electrophoresis

PV, parvalbumin

TEMED, N,N,N',N'-tetramethylethylenediamine

TnC, Troponin C

DIVALENT ION-BINDING AND THERMAL STABILITY STUDIES ON RAT β-PARVALBUMIN: EVIDENCE THAT REMOTE AMINO ACID RESIDUES INFLUENCE CD SITE ION AFFINITY

Kelly Ndubuka

Dr. Michael T. Henzl, Thesis Supervisor

ABSTRACT

Parvalbumins (PVs) are vertebrate-specific proteins (M_r 12,000), which harbor two EF-hand motifs known as the CD and EF sites. Although the CD and EF sites are typically high-affinity sites, the mammalian β-PV exhibits highly attenuated divalent ion-affinity. The physical basis for this attenuation remains unclear. A clarification of this behavior could advance our understanding of EF-hand protein structure-affinity relationships.

The question arises as to whether the difference in divalent ion-binding affinity in these proteins derives from local differences in and around the immediate binding site, or whether remote structural determinants play a role. To address this matter, site-directed mutagenesis was performed on rat β-PV at positions 49, 50, 57, 58, 59, and 60, making it identical to CPV3 at 27 of 30 residues at the CD site. Divalent ion affinity and thermal stability were evaluated for each of the variants using isothermal titration calorimetry and differential scanning calorimetry, respectively. The mutations resulted in an increase in melting temperature. However, the increases in the Ca^{2+}-free state indicating heightened stability were small in comparison to CPV3. These findings suggest that structural determinants outside the metal ion-binding motif significantly affect the attenuated binding affinity observed at the CD site in rat β-PV.

CHAPTER I

INTRODUCTION

A. Calcium as a Cellular Messenger

Calcium, the fifth most abundant element on earth, is ubiquitous in biological organisms. It plays an important role in such biological processes as nerve transmission, muscle contraction, cell motility, metabolic regulation, cell division and growth (McPhalen et al., 1991). It functions as a secondary messenger, transducing external stimuli into appropriate biochemical responses (Berridge 1993).

In eukaryotic systems, the extracellular Ca^{2+} concentration is approximately 20,000 times the intracellular concentration. The resting state Ca^{2+} cytosolic level is ~100 nM. However, following a suitable stimulus, it can increase to μM levels. This "signal" commences with activation and opening of Ca^{2+} channel proteins (Falke et al., 1994). These plasma membrane voltage-gated or ligand-gated channels permit entry of Ca^{2+} into the cytosol. The endoplasmic reticulum and mitochondria, which perform intracellular Ca^{2+} storage duties, can also release their Ca^{2+} into the cytosol (Purves et al., 2001). The resulting increase in free Ca^{2+} is transduced into a physiological response by various calcium-dependent regulatory proteins. The signal is terminated by removal of Ca^{2+} from the cytoplasm by Ca^{2+}-ATPases (Falke et al., 1994). It has been suggested that the reason the elevated calcium signal is limited to brief spikes even in non-excitable cells is due to the fact that prolonged elevation of calcium can be toxic and may lead to a variety of pathological conditions including hypertension, atherosclerosis, transformation,

malignant hyperthermia, and possible neural disorders such as spreading depression and manic-depressive illness (Berridge, 1993).

B. EF-Hand Proteins

This large class of Ca^{2+}-binding proteins is distinguished by its characteristic metal ion-binding motif, which consists of a central binding loop and flanking helical segments. This H-L-H motif is called the EF-hand because the arrangement can be mimicked with three fingers of the right hand the index, thumb and forefinger of the right hand (Figure 1-1). The index finger represents the E-helix, the forefinger the divalent-binding loop, and the thumb the F-helix (Moncrief et al., 1990). EF-hand motifs commonly occur in pairs, related by an approximate two-fold symmetry axis (Moews and Kretsinger, 1975). EF-hand proteins can serve either regulatory or buffer roles.

Calmodulin (CaM) and Troponin C (TnC) are notable examples of Ca^{2+}-dependent regulators. Calmodulin (CaM) regulates a number of fundamental cellular activities, such as cyclic-nucleotide and glycogen metabolism, intra-cellular motility and Ca^{2+}-transport. It performs these functions by mediating the activities of various target proteins such as kinases, phosphatases, metabolic enzymes and transcription factors (Carafoli and Klee, 1999). TnC is the regulatory portion of the three-component protein, troponin. The skeletal muscle isoform binds Ca^{2+} in four EF-hand motifs, two high-affinity sites and two low-affinity sites. The high-affinity sites bind Ca^{2+} and Mg^{2+} competitively with $K_{ca} \approx 2 \times 10^7\ M^{-1}$ and $K_{mg} \approx 5 \times 10^3\ M^{-1}$. The low-affinity sites preferentially bind Ca^{2+} with a $K_{ca} \approx 3 \times 10^5\ M^{-1}$(Ebashi et al 1968).

C.1. Anatomy of the EF hand

The EF-hand is a 30-residue sequence that forms a helix-loop-helix structural motif (Kretsinger and Nockolds, 1973). Residues 1-10 form the N-terminal helix; residues 10-21 form the divalent ion-binding loop; residues 19-29 form the C-terminal helix (Figure 1- 2).

Both helices are amphipathic in nature; the apolar residues facilitate formation of the EF-hand domain and help to stabilize it (Monera et al., 1992). The binding loop *per se* begins with a three-residue β-turn and ends with the three amino-terminal residues of the second α-helix (Strynadka and James, 1989).

Ca^{2+} is coordinated by ligands positioned at the vertices of an octahedron. The ligands are denoted by the axes of a Cartesian coordination system (Figure 1-3a). The *–y* ligand is a main chain carbonyl. At position *+x*, a nearly invariant aspartate furnishes an oxygen at one vertex, at the opposing *–x* vertex, a water molecule or glutamate supplies an oxygen (Strynadka et al., 1989; Falke et al., 1994). At position *-z*, a nearly invariant glutamate, coordinates Ca^{2+} in bidentate fashion. As a result, the coordination is pentagonal bipyramidal. Each ligand is approximately 2.4 Å from the central Ca^{2+}. Mg^{2+} is coordinated identically, except that the *–z* glutamate functions as a monodentate ligand. As a result, the Mg^{2+} coordination geometry is pseudo-octahederal (Strynadka and James, 1989; Henzl et al., 1999).

Due to structural constraints, positions 6 and 8 are highly conserved. The loop must change direction at position 6 to allow Ca^{2+} coordination by the side-chain at position 5 and the main-chain carbonyl at position 7. The presence of glycine at position 6 permits the required φ, ψ angles of 90° and 0°, respectively. A hydrophobic residue,

usually isoleucine, at position 8 anchors the binding loop to the hydrophobic core. The carbonyl of this residue participates in β-sheet H-bond interactions with the adjacent Ca^{2+}-binding loop (Herzberg and James, 1985). This interaction is critical for the stability of the Ca^{2+}-binding protein and for the helices that border the Ca^{2+}-binding loops (Monera et al., 1990).

C. 2. EF-Hand Specificity

Within the EF-hand protein family, there are two separate types of Ca^{2+}-binding sites, distinguished by their affinities for Ca^{2+} and Mg^{2+} (Haiech et al., 1979; Kretsinger 1980; Pauls et al., 1996a). Ca^{2+}/Mg^{2+} sites, also called "mixed sites", exhibit high affinity for Ca^{2+} ($K_{Ca} = 10^7$-10^9 M^{-1}) and moderate affinity for Mg^{2+} ($K_{Mg} = 10^3$-10^5 M^{-1}). Ca^{2+}-specific sites, on the other hand, exhibit moderate affinity for Ca^{2+} ($K_{Ca} = 10^5$ -10^7 M^{-1}) and low affinity for Mg^{2+} (K_{Mg} values of 10^1-10^2 M^{-1}).

At resting state Ca^{2+} levels, mixed sites are occupied by Mg^{2+}. However, following cellular stimulation and the subsequent increase in Ca^{2+} level, the bound Mg^{2+} is replaced by a Ca^{2+}. This competition between Ca^{2+} and Mg^{2+} is a significant factor in calcium buffering and transport within the cells (Pauls et al., 1996a; Celio et al., 1996; Henzl et al., 1998). By contrast, Ca^{2+}-specific sites are unoccupied at resting-state Ca^{2+} levels. As a consequence, they are poised to bind $Ca^{2+}$with rise in intracellular levels. These sites are well suited for Ca^{2+}-dependent regulatory functions (Haiech et al., 1979; Haiech et al., 1981; Celio et al, 1996; Pauls et al., 1996a).

D.1. Parvalbumin Tertiary Structure

Carp parvalbumin established the EF-hand structural paradigm (Krestinger and Nocknolds, 1975). Its tertiary structure includes a 40-residue N-terminal region known as the AB domain fused to a 70-residue CD-EF metal ion-binding domain. The AB domain is a vestigial EF-hand motif, rendered inactive by a two-residue deletion in the Ca^{2+}-binding loop. The A and B helices are separated by an extended eight-residue loop. The CD-EF domain includes four α-helical segments designated by the letters C through F.

Divalent ions are bound in the loops connecting the C and D helices and the E and F helices. Accordingly, these divalent ion-binding sites are called the CD and EF sites respectively (Figure 1-3b). They are spatially related by a two-fold rotation axis. The two sites are physically linked via two anti-parallel β-sheet hydrogen bonds, the only β-sheet secondary structure present in the molecule. All four helices flanking the Ca^{2+}-binding sites are amphipathic. They pack with their hydrophobic sides inside, away from the solvent, forming a central hydrophobic core. The central core consists of a number of intra- and inter-helical hydrophobic interactions.

The Ca^{2+}-binding domain has been likened to a cup, the interior lined with hydrophobic residues, the base containing the Ca^{2+}-binding loops with the outer surface and rim comprised of polar residues, charged and uncharged. The N-terminal AB domain folds over and fills the cup with its hydrophobic residues (Strynadka and James, 1989). Parvalbumins contain numerous acidic (23-27) and phenylalanine residues (8-10), but few tryptophan, tyrosine, histidine, proline, cysteine, or methionine residues. (Pechere et al., 1973; Kretsinger, 1980)

D.2. Parvalbumin Sublineages

Approximately 425 million years ago, the parvalbumin family diverged into α- and β-sublineages. They can be distinguished by isoelectric point ($\alpha \geq 5$) and several lineage-specific sequence assignments—e.g., Cys-18 and Phe-66 in β (Goodman, and Pechere, 1977; Nakayama et al., 1992). Additionally, the C-terminal F helix is typically one residue longer in α-PV isoforms. However, there are several β-PV isoforms having C-terminal extensions of more than one residue. The distribution of PVs within tissues is wide and varies among species. Birds for example express multiple isoforms in extra-muscular tissue, however in mammals β-expression is far more limited with expression in postnatals, apparently restricted to the outer hair cells of the Organ of Corti, highly specialized cells of the auditory organ that function in amplification of weak acoustic signals (Henzl and Graham, 1999).

D.3. Function

Parvalbumins are believed to primarily function as Ca^{2+} buffers, but their entire function has not been fully delineated. Although parvalbumins typically harbor Ca^{2+}/Mg^{2+}sites, consistent with a Ca^{2+}-buffering role, select parvalbumins contain a Ca^{2+}-specific site. This raises the possibility that certain parvalbumins may function as Ca^{2+}-dependent regulatory proteins (MacManus et al., 1984; Hapak et al., 1989; Cox et al., 1990 Blum and Berchtold, 1994; Henzl et al., 1998). The mammalian-β isoform, oncomodulin, was recently shown to stimulate axonal elongation in retinal ganglion cells (Yin et al., 2006). The avian β parvalbumins, avian thymic hormone (ATH) and

parvalbumin 3 (PV3), are believed to influence T-cell differentiation and proliferation (Novak et al., 1996; Novak et al., 1997).

Although abundant in select skeletal muscles fibers, parvalbumins are not found in cardiac or smooth muscle (Strynadka et al., 1989). It should be noted that Haiech et al., (1979), has proposed a mechanism for the relaxing function of PV in skeletal muscle.

The affinity of PV for Ca^{2+} exceeds that of TnC. Nevertheless, in the muscle fiber, upon release of Ca^{2+} from the sarcoplasmic reticulum, Ca^{2+} is preferentially bound by TnC. Recall that, in the resting state, parvalbumin metal ion-binding sites are occupied by Mg^{2+} and therefore unavailable for binding Ca^{2+}. After a period of roughly 100 milliseconds, however, Mg^{2+} dissociates. The vacant PV sites then successfully compete for the TnC-bound Ca^{2+}, enabling relaxation to occur.

E. Mammalian Parvalbumin Isoforms

There is an evolutionary trend to fewer parvalbumin isoforms. Fish and amphibians express multiple isoforms in a developmentally regulated pattern (Pechere et al., 1971; Simonides and van Hardeveld, 1989). The mammalian genome however, encodes one α-parvalbumin and β-parvalbumin (Fohr et al., 1993). In rats, these parvalbumins exhibit 49% sequence identity and possess virtually superimposible backbones (Ahmed et al., 1993) (Figure 1-4).

E.1. α–Parvalbumin

Rat α-parvalbumin has a net charge of -7 (pI > 5.0) and is less acidic than rat β-parvalbumin (pI 5.1 vs 3.9). It is also one residue longer than rat β-parvalbumin at the C-

terminal CD-EF domain (109 residues). Unlike rat β-parvalbumin, rat α-parvalbumin does not contain low-affinity calcium sites. The CD and EF sites of rat α-PV are mixed calcium-magnesium sites which exhibit high-affinity for calcium (K_{Ca} = ~1.6 x 10^8 M^{-1}) and moderately high affinity for magnesium ($K_{Mg} < 10^4$ M^{-1}).

α-parvalbumin is highly abundant in fast-twitch skeletal muscle fibers and rapidly-firing GABA-ergic neurons. It has also been detected in adipose tissue, testes, kidneys, skin, and the inner hair cells of the organ of Corti (Muntener et al., 1995; Schwaller et al., 1999; Pack and Slepecky, 1995; and Caillard et al, 2000).

It has been suggested that α-parvalbumin can mediate the transfer of Ca^{2+} from myofibrils to the sarcoplasmic/endoplasmic reticulum, facilitating muscle relaxation and neuronal de-excitation (Briggs, 1975; Gerday and Gillis, 1976; Haiech et al., 1979; Gillis et al., 1984). Evidence suggests that the rate of decay of calcium transients after electrical stimulation of rat skeletal muscle fibers is proportional to α-parvalbumin concentrations in the cell. In addition, ectopic expression of parvalbumin, resulting from the injection of parvalbumin cDNA into the slow-twitch muscles of rat, increases the relaxation rate in these muscle types (Muntener et al., 1995).

E.2. β-Parvalbumin

The mammalian β-isoform was first discovered in the extracts of rat hepatomas in 1978 (MacManus et al., 1978). It was called "oncomodulin" (OM) on the basis of its expression in neoplastic tissues and a purported ability to stimulate cAMP phosphodiesterase. As it turns out, the name is a misnomer. Expression in tumors and transformed cell lines is restricted to the rat. In that species, a viral promoter has been

inserted into the DNA just upstream of the oncomodulin transcription start site (Furter et al., 1989). Additionally, the early oncomodulin preparations were contaminated by trace levels of calmodulin. In fact, oncomodulin lacks the capacity to stimulate cAMP phosphodiesterase (Clayshulte et al., 1992).

The normal site of expression of the β-isoform was unknown until 1995 when it was detected in the outer hair cells of the organ of Corti (Senarita et al., 1995; Henzl et al., 1997; Thalman et al., 1998; Sakaguchi et al., 1998). Recently, Yin et al. (2006), showed that OM is also expressed in macrophages and secreted by activated macrophages into the extracellular medium, where it functions as a potent nerve growth factor.

Rat β-parvalbumin has a net charge of -15 and is more acidic (*p*I 3.9) than the α-isoform, and is shorter by one residue (108) (MacManus and Whitfield, 1983). It exhibits a much lower affinity for calcium (k_{1Ca} = 2.22 x 10^7 M^{-1}; K_{2Ca} = 1.25 x 10^6 M^{-1}) and magnesium ($K_{Mg} \approx$ 9,000 M^{-1}; $K_{Mg} \approx$ 150 M^{-1}). The EF site is a high affinity mixed-calcium/magnesium site; the CD binding site is a calcium-specific site (Hapak et al., 1989; Cox et al., 1990).

Signal transduction in the auditory organ is accomplished by alterations of a standing K^+ current across the sensory hair cells. The inner hair cells convey the signals to the central nervous system, and the outer hair cells provide a decidedly selective mechanical amplification of the signal. Outer hair cells react to changes in their membrane potential by undergoing a succession of contraction and elongation. This "electromotile response" is believed to augment the passive vibration of the basilar membrane (Dallos et al., 1997; Thalmann et al., 1998; Zheng et al., 2000). The role of

oncomodulin in the outer hair cells of the organ of Corti is unknown. It could very well function as a specialized calcium buffer, but there has also been speculation that the protein is a tissue-specific calcium-dependent regulatory protein, although a target molecule has yet been identified (Henzl et al., 1998; Thalman et al., 1998).

F. Avian Parvalbumins

Birds express two β-parvalbumin isoforms and a single α-parvalbumin. The α isoform is highly expressed in fast-twitch skeletal muscle (Heizmann and Strehler, 1979). In 1989, Brewer et al., identified a thymus-specific protein known as avian thymic hormone (ATH). Another thymic parvalbumin has since been identified and is called chicken parvalbumin 3 (CPV3)—the third parvalbumin isoform detected in chicken tissue (Hapak et al., 1994). ATH and CPV3 both belong to the β-PV sub-lineage, based upon their pI values (4.3 and 4.6 respectively), and the presence of β-lineage specific Cys-18 and Phe-66 amino-acid residues. These two PVs have been implicated in avian immune functions (Hapak et al., 1996). Recent evidence has shown that ATH is expressed at high levels in avian retina and sclera tissues (Rada and Denis, 2003), and that CPV3 is expressed in avian and amphibian auditory sensory cells (Heller et al., 2002).

G. Variation in Parvalbumin Divalent Ion-Affinity

Parvalbumins usually possess two high-affinity sites that are indistinguishable in titrations with Ca^{2+} and Mg^{2+}. However, there are exceptions to this rule. In particular, the β-PV sublineage exhibits a spectrum of divalent ion-affinity. ATH exemplifies the

high-affinity extreme exhibiting Ca^{2+}-binding constants greater than or equal to 10^8 M^{-1} for both sites (ΔG_{Ca} = -22 kcal/mol) and Mg^{2+} constants well in excess of 10^4 M^{-1}. The mammalian β-isoform (OM) occupies the low-affinity extreme. Relative to ATH, the Ca^{2+}-binding constants for the CD and EF sites in rat β-PV are decreased by factors of 70 and 10, respectively, in 0.15 M NaCl, 0.025 M Hepes, Ph 7.40 (ΔG = -18 kcal/mol) (Henzl et al., 2000). CPV3 exhibits intermediate affinity, 1.9 kcal/mol less favorable than ATH and 2.0 kcal/mol more favorable than rat β-PV.

Despite intense scrutiny, the physiological basis for these variations is incompletely understood. Initially, the differences were believed to be due to sequence differences within the ion-binding loop. For example, OM is the only PV isoform to have aspartate at position 59; all others express glutamate. Structural analysis of rat β indicates the shorter aspartyl side-chain cannot directly coordinate the bound divalent ion. Instead, a water molecule serves as the proximal ligand, and the Asp-59 carboxylate functions as the outer sphere ligand.

It was previously speculated that this single difference at position 59 was responsible for the attenuated divalent-ion affinity observed in the CD site. However, replacement of Asp-59 with glutamate in rat β, produced a minimal increase in Ca^{2+} affinity ($\Delta\Delta G_{Ca}$ = -0.1 kcal/mol). Interestingly, the reverse mutation, a substitution of Glu-59 with aspartate, induced a significant decrease in Ca^{2+} affinity in rat α ($\Delta\Delta G_{Ca}$ = 1.7 kcal/mol) (Henzl et al., 2004).

There is accumulating evidence that structural features remote from the binding site influence divalent ion-binding properties. The Henzl lab recently compared the Ca^{2+}-binding properties of isolated rat α- and β CD-EF domains. Whereas the standard Ca^{2+}-

binding free energies for the intact proteins differ by 3.5 kcal/mol in Hepes-buffered saline, the isolated metal ion-binding domains differ by just 1.4 kcal/mol (Henzl et al., 2003).

This observation, suggested that the AB domain influenced Ca^{2+} affinity. Additional examination of the AB/CD-EF interaction employed isolated AB and CD-EF fragments from rat α and β (Henzl et al., 2004). Significantly, the βCD-EF domain exhibits higher affinity for αAB domain than for the βAB domain at saturating Ca^{2+} levels. Consistent with that finding, the αAB/βCD-EF complex binds Ca^{2+} more tightly than the homologous β/β complex. Evidently, the AB domain is an important determinant of parvalbumin divalent ion-binding properties (Henzl et al., 2003).

H. Thesis Objectives

Rat β-PV and CPV3 display 70% sequence identity (Figure 1-5). Despite this similarity in primary structure, they exhibit distinctly different divalent ion-binding properties. In Hepes-buffered saline at 25 ˚C, the difference in Ca^{2+} affinity (2.0 kcal/mol) is largely a reflection of the behaviors of the CD sites in these two proteins. The question arises as to whether this difference is due solely to sequence nonidentities in the CD site *per se* (residues 41 -70) or whether it is also a consequence of structural differences elsewhere in the molecule. This study was undertaken to address this question.

We recognized that replacement of residues 49, 50, 57, 58, 59, and 60 in rat β-PV with the corresponding amino-acids from CPV3 would produce a protein identical to CPV3 at 27 of 30 residues in the CD site. Moreover, the remaining differences would be

highly conservative. The extent to which the resulting variant of rat β–PV imitated CPV3 would furnish insight into the relative importance of structural factors remote determinants from the CD site.

Thus OM → CPV3 mutations were performed at these six residues and performed in four stages. Initially phenylalanine (F) at position 49 and Isoleucine (I) at position 50 were replaced by isoleucine and leucine, respectively (variant I F49I/I50L), in addition to this, tyrosine (Y) at position 57 and leucine (L) 58 were substituted with phenylalanine (F) and isoleucine (I) respectively (variant II, F49I/I50L/Y57F/L58I). Aspartate (D) at position 59 was replaced with glutamate (E) (variant III, F49I/I50L/Y57F/L58I/D59E) and finally glycine (G) at position 60 was substituted with glutamate (E) (variant IV, F49I/I50L/Y57F/L58I/D59E/G60E). These four proteins were analyzed by ITC and DSC to ascertain the impact of these residues of divalent ion-affinity and protein stability.

Figure 1-1: a) The EF-hand binding site containing a calcium ion coordinated by 7 oxygen ligands. b) The three dimensional structure of the EF-hand simulated by the right hand, with the extended thumb and the index finger representing the α–helices and the bent middle finger indicating the Ca^{2+}–binding loop.

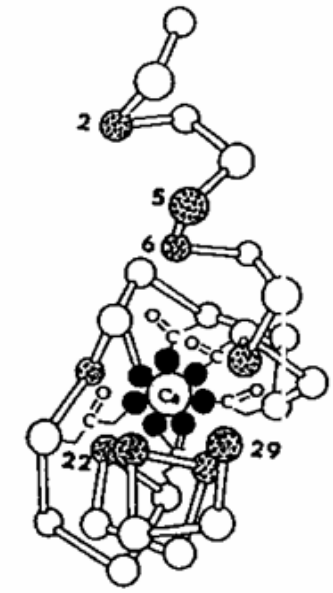

a

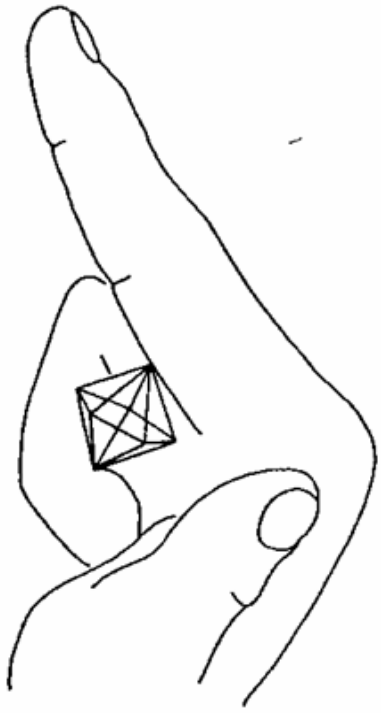

b

Figure 1-2: The canonical EF-hand consisting of two α-helices flanking a 12-residue calcium-binding loop.

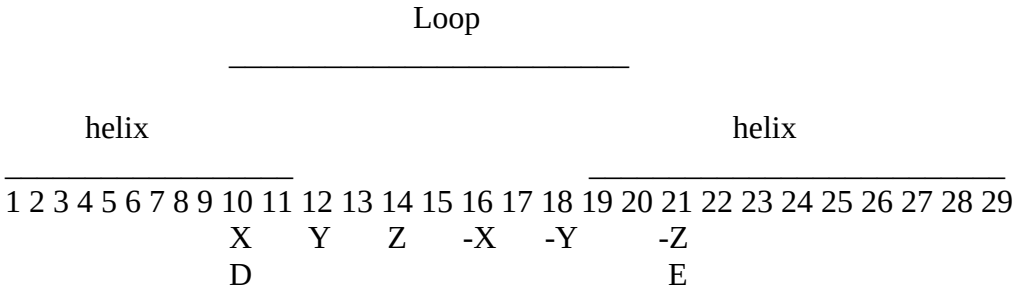
Loop
helix
helix
1 2 3 4 5 6 7 8 9 10 11 12 13 14 15 16 17 18 19 20 21 22 23 24 25 26 27 28 29
X
Y
Z
-X
-Y
-Z
D
E

Figure 1-3: EF-hand motif Ca^{2+} ligand Cartesian coordination and its three dimensional representative structure

A. The canonical EF-hand metal ion-binding motif, showing the pseudo-octahedral arrangement of ligands around the bound Ca^{2+}. The coordination of the glutamyl residue at *–z* is bidentate, so that the ligand geometry is actually pentagonal bipyramidal. A water molecule (cyan) occupies the *–x* position. The *–y* ligand, an invariant main-chain carbonyl, is obscured in this view.

B. Rat β-parvalbumin tertiary structure, produced from the 1RRO PDB file. The N-terminal AB domain (residues 1-39) occludes the hydrophobic face of the CD-EF metal ion-binding domain (41-70). The Divalent ions are bound by the EF-hand sites of the CD-EF domain.

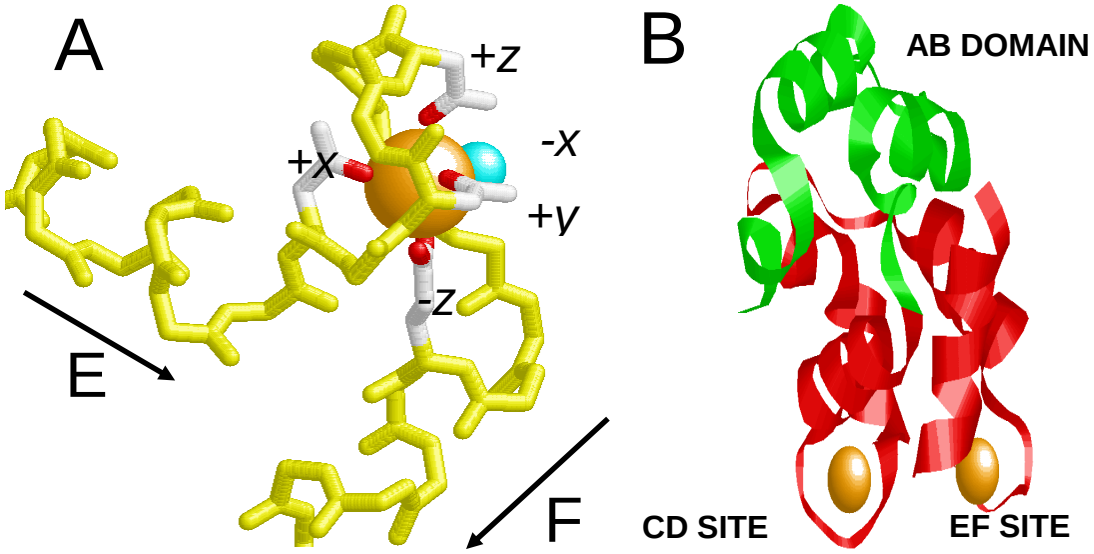
A
+z
-x
+x
+y
-z
E
F
B
AB DOMAIN
CD SITE
EF SITE

Figure 1-4: Superimposed peptide backbones of Ca^{2+} bound rat α- and β-PV.

Superimposed peptide backbones of Ca^{2+}-bound rat α- and β-parvalbumin

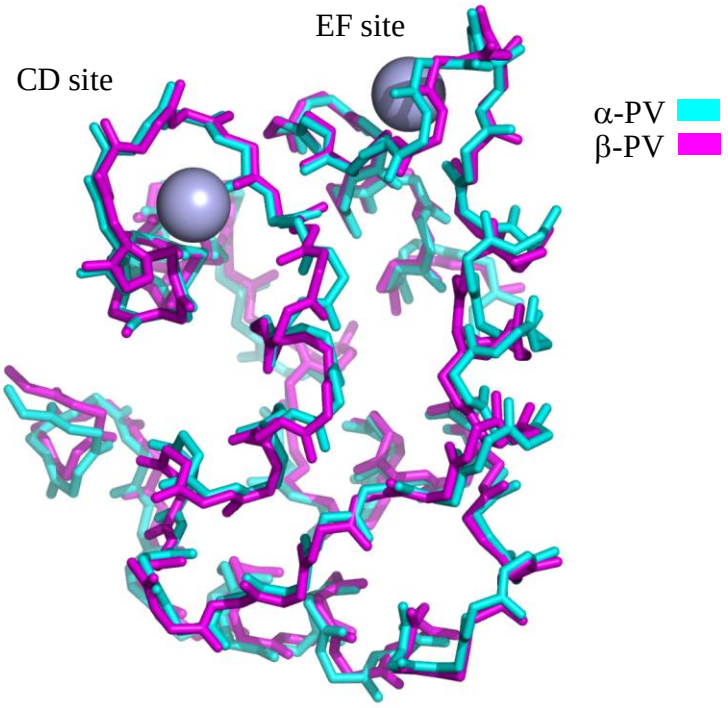

The average RMSD is 0.8 Å

Figure 1-5: Amino acid sequences of rat β-PV and CPV3

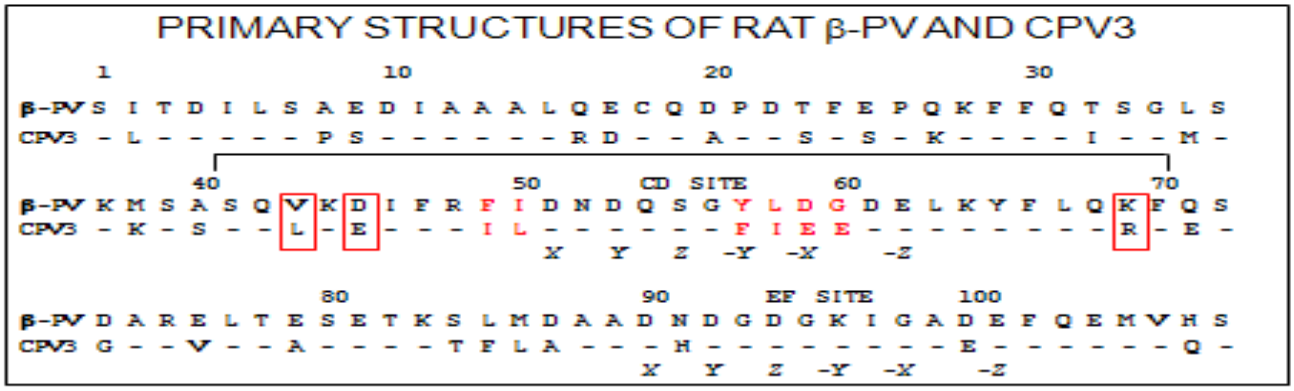

The dashes indicate conserved amino acids. The CD site runs from position 51 to 62. The red indicate conservative differences between the two proteins.

CHAPTER II

Experimental Procedures

A. Materials

- Agarose (Molecular biology grade), acrylamide, EDTA (free acid), lysozyme, ethidium bromide, TEMED, sodium acetate, bromophenol blue, coomassie brilliant blue R-250, DEAE-Sepharose CL-6B, and Sephadex G-75 were purchased from Sigma Aldrich Chemical Company.
- $CaCl_2$, $MgCl_2$, DTT, ampicillin, EDTA disodium salt, LB agar (Miller), LB broth (Miller), acetic acid, hydrochloric acid (certified), sodium hydroxide (certified), sodium chloride, potassium chloride, Tris (crystallized free base) and HEPES (enzyme grade) were obtained from Fisher-Scientific.
- Ethanol and methanol were obtained from the University of Missouri-Columbia Chemistry stores.
- Oligonucleotides used in the site-directed mutagenesis were obtained from Integrated DNA Technologies.
- Ultrafiltration cell and ultrafiltration membrane (PM10) were provided by Amicon Inc.
- Spectrapor I dialysis tubing (MWCO 6-8,000) was purchased from Spectrum Laboratories.
- Affi-gel 10 was purchased from Bio-Rad.
- Wizard plasmid purification kit and DNA extraction kit were obtained from Promega.

B. BUFFERS

- Hepes-buffered Saline (HBS) solution:

0.15 M NaCl,

0.025 M Hepes, pH 7.40

- Sample buffer for Polyacrylamide Gel Electrophoresis (3X)

30% glycerol

0.186 M Tris-HCL (PH 8.0)

0.15% bromophenol blue

3% 2-mercaptoethanol

C. Methods

C.1. Mutagenesis

The 49/50/57/58/59/60 variant was produced from 49/50/57/58/59 using oligonucleotides supplied by Integrated DNA Technologies (Coralville, IA) and the Quik-Change mutagenesis kit (Stratagene). DNA isolated from small-scale (5 ml) cultures of transformants using the Promega Wizard kit. The DNA samples were submitted to the University of Missouri-Columbia DNA Core facility for sequencing to verify the presence of the mutation and the fidelity of the coding sequence. Isolation and purification of these proteins is described as follows.

C.1.a Lysis

A 25 ml LB culture supplemented with 300 µg/ml ampicillin was inoculated with a single colony and incubated overnight at 37°C with shaking (250 rpm). The following day, four 1-L LB/amp cultures were each inoculated with 5 mL of the starter culture. Incubation was continued at 37°C with agitation for 24 hrs. The cells were collected by centrifugation at 4200 rpm for 30 min in a Beckman J6B centrifuge. The cell paste was resuspended in 5 volumes of 20 mM Hepes, pH 7.4, and then subjected to a freeze-thaw cycle to promote disruption of the cell membrane. Upon thawing, a hen egg lysozyme solution (20 mg/mL in 20 mM Hepes, ph 7.4) was added to the cell suspension to yield 5 mg lysozyme per gm of cell paste. Following incubation at 37°C for 20 min, the resulting viscous preparation was passed through a French pressure cell.

C.1.b Heat Treatment.

After adding $MgCl_2$ and $CaCl_2$ to final concentrations of 10mM and 1mM, respectively, the crude lysate was heated to 78-80°C in a boiling water bath and maintained at that temperature for 5 min with continuous agitation. After cooling on ice, the resulting suspension was clarified by centrifugation in 40 ml centrifuge tubes at 27,000 x g for 30min at 4°C. All subsequent purification steps were performed at this temperature.

C.1.c Anion–Exchange Chromatography (DEAE Sepharose)

The resulting cell extract was diluted two-fold with deionized water and then loaded by gravity flow onto a DEAE column (4 ml bed volume) equilibrated with 20 mM Hepes, pH 7.4 buffer. After washing with 10 mL of buffer, the column was eluted at 0.75 mL/min with a 0–0.6 M NaCl gradient, prepared in 20 mM Hepes, pH 7.4. Column fractions containing the protein were identified by non-denaturing PAGE, concentrated to 5 ml in an Amicon ultrafiltration cell, and quick frozen in liquid nitrogen.

C.1.d Gel Filtration Chromatography (Sephadex G-75)

A 375 mL column of Sephadex G-75 was equilibrated with two bed volumes of 0.15 M NaCl, 0.025 M Hepes, pH 7.4. The protein sample was loaded onto this column and eluted at 0.75 mL/min to remove residual contaminants. 6.0 mL fractions were collected. Rat β-PV and the variants described here, exhibit characteristic UV spectra. Thus, fractions containing the desired protein could be identified by UV spectroscopy. Due to the absence of tryptophan in these proteins, the UV spectrum provides a strict measure of homogeneity. Assuming an average extinction coefficient for tryptophan 0.5 cm^{-1} $(mg/ml)^{-1}$ at 292 nm, the purity of all the preparations used in these studies was judged to exceed 98%.

Protein concentrations were determined spectrophotometrically, using molar extinction coefficients of 2880 M^{-1} cm^{-1} for wild-type rat β; 49/50, 2970 M^{-1} cm^{-1}; 49/50/57/58, 1708 M^{-1} cm^{-1}; 49/50/57/58/59, 1650 M^{-1} cm^{-1}; and 49/50/57/58/59/60, 1600 M^{-1} cm^{-1}. Extinction coefficients were measured in a Beckman XL-I analytical ultracentrifuge, employing a synthetic-boundary cell. Upon acceleration to 5,000 rpm, the

cell produces a sharp solvent-sample interface, which is examined by interference optics and UV absorbance. The deformation of the interference pattern at the interface yields the mass concentration, 3.333 fringes corresponding to a protein concentration of 1.0 mg/mL in a 1.2 cm cell.

C.2 Removal of Divalent Ions from Buffers and Protein Solutions

Divalent metal ions were removed from protein solutions and buffers prior to analysis by passage over EDTA-agarose at 4°C. This chelating matrix was prepared by addition of 5.0 g EDAC to 100 ml aminohexyl agarose in 0.5 M EDTA, pH 6.0, followed by incubation at 25°C for 1 hr with agitation. A second 5.0 g aliquot of EDAC was added, and incubation was continued for another 4 hours. The resulting material was washed with water and then with 10 mM Ca^{2+}, to remove excess EDTA. Prior to use, the gel was treated with dilute HCl (pH 2) to release bound divalent ions, then neutralized with 0.15 M NaCl, 0.025 M Hepes, pH 7.4. The Ca^{2+} binding capacity of the resulting material is 25-30 µmol/mL of gel. The aminohexyl agarose was prepared by activation with 1,4-butanedioldiglycidyl ether and followed by reaction with 1,6-diaminohexane at pH 13.

Prior to passage over the column, protein solutions were diluted to 1 mg/mL. Typically, 1-2 mL of resin was used for each milligram of protein loaded, and elution was performed at 0.5 mL/min. In every case, the residual Ca^{2+} content following this treatment was less than 0.02 molar equivalents, as determined by flame atomic absorption at 422.7 nm.

C.3 Isothermal Titration Calorimetry

All isothermal titration calorimetry (ITC) experiments were performed at 25°C in a VP-ITC calorimeter (MicroCal, Inc.). Following thermal equilibration, additions of titrant (7-10 μL) were made at 240 second intervals, to the 1.41 mL protein samples. All experiments were conducted in 0.15 M NaCl and 0.025 M Hepes-NaOH, at pH 7.4. Origin (v.5.0) version was used for integration of the raw VP-ITC data and for the analysis of individual titrations, using the curve-fitting modules supplied with the instrument. Divalent ion affinities were determined by global analysis of a suite of ITC experiments. Titrations were carried out with Ca^{2+} in the absence and presence of chelators, with Ca^{2+} at several fixed levels of Mg^{2+}, and Mg^{2+} in the absence and presence of EDTA.

All Ca^{2+} and Mg^{2+} solutions were standardized by calorimetric titration of EDTA of known concentration. These were used in turn to standardize NTA solutions. The binding properties of the chelating agents were determined by global analysis of the following experiments: $^{1}Ca^{2+}$ vs. EDTA, $^{2}Mg^{2+}$ vs. EDTA, $^{3}Ca^{2+}$ vs. EDTA in the presence Mg^{2+}, $^{4}Ca^{2+}$ vs. EGTA, $^{5}Ca^{2+}$ vs. EGTA in the presence of EDTA, $^{6}Ca^{2+}$ vs. NTA, $^{7}Ca^{2+}$ vs. NTA in the presence of EDTA, and $^{8}Ca^{2+}$ vs. NTA in the presence of EGTA. EDTA, EGTA, and NTA have Ca^{2+}-binding constants of 4.8×10^{7} and 1.7×10^{7}, and 1.2×10^{4} M^{-1}, respectively. The corresponding binding enthalpies are –6.3, –7.6, and –2.0 kcal/mol. The heat from the initial injection is invariably inaccurate, due to diffusion of the titrant into the protein solution in the cell during the thermal equilibration step. Thus, each experiment included a pre-titration injection (2 μL), which was excluded from analysis. The standard deviation for the instrument (0.35 μcal per injection) was

estimated from repeated additions of 1.0 mM Ca^{2+} into excess EDTA in 0.15M NaCl and 0.025 M Hepes NaOH at pH 7.4. This figure was applied to all data points.

After subtraction of the baseline heats, the individual experiments were compiled into a master data file. Weighted nonlinear least-squares analysis was then applied to this composite data set, varying the binding enthalpies and binding constants for Ca^{2+} and Mg^{2+} so as to minimize the reduced chi-square value $\chi_r^{2.}$ The procedure is described in detail in Henzl et al., (2003).

C.4 Differential Scanning Calorimetry (DSC)

DSC was used to resolve the energetics of conformational transitions of rat β-PV and the four variants. By measuring the temperature dependence of the partial heat capacity, DSC gives immediate access to the thermodynamic mechanism that governs a conformational equilibrium between the folded and the unfolded forms of a protein.

A solution containing the protein of study is placed in the sample cell and an equal volume of buffer solution in the reference cell and the two cells are heated at a constant rate. However, because the heat capacities of the solution in the sample cell and the reference cell differ, a certain amount of electrical power is required to zero the temperature difference between the two cells. This power difference (J s^{-1}) as a function of the scanning rate (K s^{-1}) is a direct measure of the heat capacity difference between the solution and the solvent in units of J K^{-1}.

$$\Delta C_p^{sol-solv} = C_p^{sol} - C_p^{solv} \qquad (2\text{-}1)$$

The DSC experiments were performed in a Nano-Differential Scanning Calorimeter (Calorimetry Sciences Corporation), equipped with 0.32 mL cylindrical hastalloy cells. Temperature calibration was examined with DMPC, DPPC and DSPC, using the published transition temperatures (Mabrey and Sturtevant, 1976). The accuracy of the differential power measurements was verified with internally generated electrical calibration pulses.

Samples were dialyzed against 0.15 M NaCl, 0.01 M NaPi, and 0.005 M EDTA at pH 7.4, which then served as the reference buffer. Data was collected at 60º/h. Each protein included in the study exhibited an endotherm on rescan, indicating that denaturation was reversible.

CHAPTER III

RESULTS

The sequence of rat β-PV is identical to that of CPV3 at 75 of 108 residues. The two proteins are identical within 26 of 38 residues within the AB domain. Nevertheless, rat β- PV exhibits substantially lower Ca^{2+} and Mg^{2+} affinities. This difference in divalent ion affinities is primarily reflected in the behaviors of the CD binding site. The question arises: To what extent is the disparate behavior due to amino acid substitutions in the CD site itself? Do substitutions elsewhere in the protein contribute to the different metal ion-binding properties? This project was designed to address these questions.

Within the CD domain, the sequences of rat-β-PV and CPV3 differ at positions 43, 45, 49, 50, 57, 58, 59, 60 and 69. Positions 49, 50, 57, 58, 59, and 60 were judged the most significant because they occur in or at the border of the metal ion-binding loop. Thus, this project focused on these residues. The remaining three differences occur in the flanking helices and are highly conservative: valine vs. leucine at position 43, aspartate vs. glutamate at position 45, lysine vs. arginine at position 69.

Four variant proteins were produced, denoted with Roman numerals I through IV. The individual mutations will be indicated by one letter amino-acid abbreviations followed by the sequence position number and then the amino acid abbreviation of the new amino acid residue. For example in variant I, phenylalanine at position 49 was replaced by isoleucine, and isoleucine at 50 was replaced by leucine. Variant II was derived from variant I, by introducing the Y57F and L58I mutations. The introduction of D59E mutation in variant II yielded variant III. Finally, addition of the G60E mutation to

variant III yielded variant IV. For convenience, the mutations are listed in Table 3-1. Each of the four proteins was subjected to a suite of experiments to determine their divalent-ion binding and thermodynamic properties.

A. Divalent Ion-Binding Properties

The impact of the amino acid substitutions on divalent ion-binding behavior was examined by ITC. This technique is arguably the single most powerful tool for investigating protein-ligand interaction. It provides a detailed, comprehensive analysis of the thermodynamics of the process. Free energy, enthalpy, and entropy changes, as well as binding stoichiometry, can all be derived by this single method. Enthalpy is measured directly. The association constant which yields the free energy change is estimated from the dependence of the injection heat on ligand concentration. The entropy change ($T\Delta S$) represents the difference between the enthalpy and free energy.

Microtitration calorimeters are designed to measure the heat evolved upon association of a ligand with its binding partner. The instruments contain identical reference and sample cells, both of which are housed in a jacket surrounded by an adiabatic jacket. The sample and reference cells are in intimate contact with precision Peltier modules. Minute temperature differences resulting from the binding reaction produce a voltage in these devices. This voltage is converted to power (μcal/sec).

During an experiment, aliquots of the ligand are added to the sample cell at precise intervals under computer control. Whereas a constant reference power (10-50 μW) is applied to the reference cell, a feedback circuit regulates the power applied to the sample cell. In an exothermic reaction, the temperature in the sample cell will increase,

and the feedback power will be decreased to maintain equal temperatures between the sample and reference cells. For endothermic reactions, the reverse will occur.

The heat absorbed or evolved during a calorimetric titration is proportional to the fraction of bound ligand. In the initial injections, all or most of the added ligand is bound to the macromolecule, resulting in large endothermic or exothermic signal. With subsequent additions however, as saturation of the macromolecule is approached, the fraction of added ligand that binds decreases with an accompanying decrease in the signal. Ultimately, the signal returns to baseline levels, i.e., heat associated with mixing. The cumulative heat of reaction (Q) is equal to,

$$Q = 10^6 \times \Delta H[M]_{total}.V\left(\frac{Kx}{1+Kx}\right) \qquad (3\text{-}1)$$

Where ΔH is the molar enthalpy, M is the macromolecular concentration, V is the reaction volume, K is the association constant, and x is the free ligand concentration. In ITC, however, the free ligand concentration is not known. Rather, it must be calculated from total macromolecule and ligand concentration and the current estimate of the binding constant. For single-site systems, x can be calculated analytically. For more complex systems, x must be solved for numerically (e.g., by bisection).

A.1. Global Analysis of ITC Data

At the high-affinity end, the protein concentration is too low to permit accurate heat measurements; at the low-affinity end, the reaction does not proceed sufficiently far to completion to permit accurate estimation of the binding constant. Ca^{2+} binding, with a binding constant on the order of 2.4×10^7 is too tight. Also, Mg^{2+} binding borders on

being too weak. Both of these obstacles complicate the estimation of PV divalent ion-binding properties.

One way to extend the range of ITC is through the use of competition. Competitors increase the curvature in binding isotherms, thus providing a platform for a more accurate determination of the binding parameters. (Sigurskjold et. al., 1994; Sigurskjold 2000; Henzl 2003a). The competitive chelators used in this work were nitrilotriacetic acid (NTA), ethylenediamine-tetra-acetic acid (EDTA), and ethyleneglycol-bis(β-aminoethyl ether)-N, N, N', N'-tetraacetic acid (EGTA). Under the solution conditions stated, NTA, EDTA and EGTA bind a single equivalent of calcium each with association constants of 1.17 x 10^4 M^{-1}, 4.4 x 10^7 M^{-1}, and 1.7 x 10^7 M^{-1}, respectively. They display apparent enthalpy changes of -1960 kcal/mol, -6300kcal/mol, and -7500 kcal/mol, respectively (Henzl et al., 2003a; Henzl el al., 2003).

Each protein was titrated with Ca^{2+} alone, Mg^{2+} alone, Ca^{2+} at several fixed levels of Mg^{2+}, Ca^{2+} in the presence of chelators (NTA, EDTA, EGTA), and Mg^{2+} in the presence of EDTA. The results were then compiled into a composite dataset and then subjected simultaneous or global least-squares analysis performed with a Fortran-based fitting program. In this program, integrated heats are predicted by a two-step procedure. First, the free divalent-ion concentration is estimated by employing a bisection routine to solve the mass conservation equation, given the current vector of parameter values. With knowledge of the free ligand concentration (χ), after the *j*th addition of titrant, the cumulative heat of binding (Q_j) can be calculated with the following equation:

$$Q_j = \sum_i Q_i = V_o M_T \sum_i \Delta H_i \frac{\beta_i x^i}{p} \qquad (3\text{-}2)$$

where Q_i is the heat associated with the *i*th form of the protein, V_o is the sample volume, M_T is the total macromolecule concentration ΔH_i is the molar binding enthalpy for the *i*th form, β_i is the overall macroscopic binding constant for formation of the *i*th state, and *P* is the binding partition function. The corresponding heat associated with the *j*th addition of titrant, q_j is equal to

$$qj = Q_j - Q_{j-1} + \frac{dV_j}{V_o}\left[\frac{Q_j + Q_{j-1}}{2}\right] \qquad (3\text{-}3)$$

Where, Q_j and Q_{j-1} are the cumulative heats of binding after the *j* and *j*-1 additions respectively. The third term on the right side of eq 3-3 corrects for the volume of solution displaced from the sample cell by the injection of the titrant (dV_j).

In this analysis, we are assuming that the order of occupancy observed for the wildtype protein is preserved. The following paragraphs describe the impact of the OM → CPV3 mutation for each of the four variant proteins.

Table 3-2 lists the resulting binding constants and enthalpies of all the proteins in this study for Ca^{2+} and Mg^{2+}, whereas Table 3-3 summarizes their divalent ion-binding energetics. The results indicate that the mutated CD site retaining its low affinity signature. The k_1 and k_2 headings correspond to the EF and CD binding constants, respectively.

Variant I: F49I/I50L

Least squares analysis of these data indicates that the mutation of wild-type rat β-PV at positions 49 and 50 produces an elevation in Ca^{2+} affinity at both sites. The binding constants for the EF site and CD site increase from 2.30 x 10^7 M^{-1} to 3.25 x 10^7 M^{-1}, and from 1.52 x 10^6 M^{-1} to 2.32 x 10^6 M^{-1}, respectively (Table 3-2). These changes correspond to an improvement in Ca^{2+}-binding free energy of 0.20 kcal/mol for the EF-

site, and 0.24 kcal/mol for the CD site (Table 3-3). Because the exothermicity of both binding events are decreased in variant I, the more favorable ΔG must have an entropic origin.

The effects of the mutation have a smaller impact on Mg^{2+} affinity. The Mg^{2+}-binding constant for the EF site increases from 9.23 x 10^3 to 1.35 x 10^4 M^{-1}(Table 3-2). By contrast, Mg^{2+} affinity in the CD site decreases from 1.68 x 10^2 M^{-1} to 1.46 x 10^2 M^{-1} (Table 3-2). As a result, the overall $\Delta\Delta G$ is -0.13 kcal/mol (Table 3-3). With the F49I/I50L substitution, both sites show increased endothermicity for Mg^{2+} binding relative to the wild type protein. An increase of 1.22 kcal/mol and 1.34 kcal/mol is observed for the EF- and CD-sites respectively (Table 3-3). This result suggests, as remarked for Ca^{2+}, that the entropic contribution to Mg^{2+} binding is substantially more favorable for the 49/50 variant. A representation of the divalent ion-binding behavior of β49/50 is displayed in figure 3-1.

Variant II: F49I/I50L/Y57F/L58I

This protein was produced by adding the Y57F and L58I to variant I. The calcium binding curve for β49/50/57/58 is presented in Figure (3-2 A). The mutations at positions 57 and 58 increase the Ca^{2+} binding constant for the EF site from 3.25 x 10^7 M^{-1} (49/50) to 4.29 x 10^7 M^{-1}, and reduces the corresponding CD site binding constant from 2.32 x 10^6 (49/50) to 1.5 x 10^6 M^{-1} (Table 3-2). However, like variant I, this protein displays an overall improvement in Ca^{2+} binding free energy relative to wild type. The $\Delta\Delta G$ (0.36 kcal/mol) is comparable to that observed for 49/50 (0.44 kcal/mol) (Table 3-3). However, this improvement is entirely due to increased affinity at the EF site. In fact, the ΔG

associated with Ca^{2+} binding at the CD site is essentially unchanged at ($\Delta\Delta G$ = +0.01 kcal/mol) (Table 3-3).

Although 49/50 and 49/50/57/58 have comparable overall Ca^{2+} affinity, the latter has significantly higher affinity for Mg^{2+} (Table 3-3). In addition, unlike Ca^{2+}, the affinity for Mg^{2+} also improves at both sites (Table 3-3). The binding constant for Mg^{2+} at the EF-site increases from 1.35 x 10^4 (49/50) to 1.79 x 10^4 M^{-1}, and the CD site increases from 1.46 x 10^2 (49/50) to 3.34 x 10^2 M^{-1} (Table 3-2). The magnesium binding curve for β49/50/57/58 is presented in Figure (3-2 B). As a result, variant II displays a greater improvement in Mg^{2+} binding, relative to wildtype β-PV than does variant I (-9.24 *vs.* -8.57 kcal/mol (Table 3-3)). The overall improvement in ΔG_{Mg} for 49/50/57/58 is +0.80 kcal/mol, as compared to -0.13 kcal/mol for 49/50 (Table 3-3).

Variant III: F49I/I50L/Y57F/L58I/D59E

Production and research on this variant was performed by Dr. M. T. Henzl.

This variant was produced by a D59E substitution in variant II. Upon direct titration with Ca^{2+}, this variant produced results agreeable to a single-site model with an apparent binding constant of 5.7 x 10^5 M^{-1}. Global analysis, however, indicates the presence of a second binding event with a small ΔH. This second binding event is visibly apparent in competition experiments with Ca^{2+} in the presence of NTA (Figure 3-3A, □ and△). Other competing ligands EDTA, EGTA and Mg^{2+}, provide additional evidence for the second binding event (Figure 3-3 B, C, and D). However, the second binding event is less visible when these competitors are used in comparison to NTA. The global

analysis yields indicate Ca^{2+}-binding constants of 4.65 x 10^7 and 1.70 x 10^6 M^{-1} (Table 3-2)

Least squares analysis indicates that the introduction of D59E into variant 49/50/57/58 gives rise to a mere ΔG_{ca} of -0.12 kcal/mol (Table 3-3). The binding enthalpies however, have undergone significant changes, with $\Delta\Delta H_{ca}$ values for the EF and CD sites at -1.14 kcal/mol and 3.54 kcal/mol, respectively (Table 3-3).

Mg^{2+} binding in variant III is more favorable when compared to variant II. The $\Delta\Delta G$ associated with Mg^{2+} binding is 0.29 kcal/mol more favorable than that for 49/50/57/58 (Table 3-3). Most of this change is attributable to an increase in the CD site binding constant from 3.34 x 10^2 to 5.09 x 10^2 M^{-1}(Table 3-2). The EF site value is nearly unchanged at 1.92 x 10^4 M^{-1} vs 1.79 x 10^4 M^{-1} (Table 3-2). The binding enthalpy for Mg^{2+} is more favorable ($\Delta\Delta H$ = -0.89kcal/mol) for the EF site and less favorable ($\Delta\Delta H$ = - 1.11 kcal/mol) for the CD site (Table 3-3).

Variant IV: **F49I/I50L/Y57F/L58I/D59E/G60E**

ITC data for 49/50/57/58/59/60 reveal a remarkably large endothermic value for the second binding event (Figure 3-4), despite the fact that this variant exhibits an overall Ca^{2+} binding affinity greater than wildtype (Table 3-3). Typically, parvalbumins exhibiting endothermic Ca^{2+}-binding events, display attenuated divalent ion affinity (Henzl et.al., 2004). However, in this case 49/50/57/58/59/60 shows a $\Delta\Delta G_{Ca}$ of 0.58 kcal/mol and a $\Delta\Delta G_{Mg}$ 1.03 kcal/mol improvement over wildtype (Table 3-3).

Least-squares analysis indicates that the introduction of G60E into 49/50/57/58/59 reduces the EF-site Ca^{2+}-binding constant from 4.65 x 10^7 to 3.86 x 10^7 M^{-1} and increases

the CD site affinity from 1.7 x 10^6 to 2.44 x 10^6 M^{-1} (Table 3-2). These compensating changes leave the overall ΔG largely unaffected ($\Delta\Delta G$ = -0.1 kcal/mol) (Table 3-3). As with variant III, the slight free energy change is the consequence of large, opposing changes in binding enthalpy and entropy.

The $\Delta\Delta H_{Ca}$ values for the EF and CD sites are 0.93 and 2.43 kcal/mol (Table 3-3), respectively. In the case of Mg^{2+} binding, the mutation slightly lowers the affinity at the EF site from 1.92 x 10^4 to 1.72 x 10^4 M^{-1}, and leaves affinity at the CD site virtually unchanged (5.11 x 10^2 *vs* 5.09 x 10^2 M^{-1}) (Table 3-2). This gives rise to an overall $\Delta\Delta G$ of 0.06 kcal/mol (Table 3-3). The $\Delta\Delta H_{Mg}$ values for the EF and CD sites are 0.76 and 0.53 kcal/mol, respectively (Table 3-2).

B. Analysis of DSC Data.

A baseline, obtained with sample and reference cells filled with buffer, was subtracted from the protein data prior to analysis. The resulting heat capacity data, c_p, with units of mcal/K, were analyzed with the following model.

$$cp = \left(\frac{10^3 mc.V}{MW}\right)\left(\left[\Delta H_c(T_m) + \beta\Delta C_p(T - T_m)\right]\left[\frac{\Delta H_{vH}(Tm) + \Delta C_p(T - Tm))}{RT^2}\right]\left(\frac{K(T)}{(1+K(T))^2}\right) + \left(\frac{K(T)}{1+K(T)}\right)\Delta C_p + c_{p,n} + \left(\frac{1}{1+K(T)}\right)(b.(T - T_m)) + \left(\frac{K(T)}{1+K(T)}\right)(d.(T - T_m))\right) \quad (4\text{-}4)$$

Where, *mc* is the protein concentration in g/L, *V* is the sample cell volume in L, *MW* is the protein molecular weight, and β is the ratio of the calorimetric and van't Hoff

enthalpies (ΔH_c and ΔH_{vh}, respectively). ΔC_p is the change in heat capacity that sometimes accompanies denaturation (assumed to be temperature-independent), T is the absolute temperature, T_m is the melting point or transition mid point, R is the gas constant and $K(T)$ is the temperature-dependent equilibrium constant.

$$K(T) = \exp(-\Delta G(T)/RT) \qquad (4\text{-}5)$$

Where $\Delta G(T)$ is given by the Gibbs-Helmholtz equation:

$$\Delta G(T) = \Delta H\left(\frac{T_m - T}{T_m}\right) + \Delta C_p\left[(T - T_m) - T\ln\left(\frac{T}{T_m}\right)\right] \qquad (4\text{-}6)$$

For a two-state transition, the fractions of native and denatured material equal $1/(1 + K(T))$ and $K(T)/(1 + K(T))$, respectively.

The first two terms in eq 4-4 describe the peak in the heat capacity function and the accompanying baseline shift, respectively. The third term, $c_{p,n}$, represents the value of the native state heat capacity at the T_m, and the remaining two terms describe the temperature dependence of the native and denatured state heat capacities, respectively.

DSC data in Figure 3-5 displays the molar heat capacities of the wild-type, and four variant proteins. The four variant proteins exhibited increased ΔH_{cal} values in comparison to wild-type rat β-PV. These proteins also exhibit elevated melting temperatures, with ΔT_m values ranging from 1.9˚ to 3.4˚ (Table 3-4). Interestingly, F49I/I50L, the protein most similar to wild-type, displayed the greatest increase in T_m. The double substitution also increases the calorimetric enthalpy of rat β-PV by 13.7 kcal/mol (Table 3-4).

Introduction of Y57F and L58I into variant I, to produce variant II, causes the melting temperature to diminish by 1.5˚ and leaves ΔH_{cal} relatively unchanged ($\Delta\Delta H_{cal}$ = 0.4 kcal/mol).

Recall that the ITC analysis of variant III (F49I/I50L/Y57F/L58I/D59E) revealed that the mutations caused a marked decrease in the exothermicity of the second binding event, along with a small increase in Ca^{2+}-binding affinity. DSC analysis of this variant protein indicates an improvement of 2.3˚ (Table 3-4) in thermal stability, relative to wild type rat β-PV. However, in comparison to variant II, the replacement of Asp-59 by glutamate raises the melting temperature by a mere 0.4˚.

Introduction of G60E into 49/50/57/58/59 produced an additional endothermic change in the enthalpy change for the second Ca^{2+}-binding event. In the DSC analysis, the mutation reverses the impact of the D59E mutation, returning the T_m to to 51.2 ˚C (identical to the T_m for VarII = 51.2 ˚C).

Table 3-1: The variant proteins and their corresponding mutations.

Variant	*Mutation*
Variant I	F49I/I50L
Variant II	F49I/I50L/Y57F/L58I
Variant III	F49I/I50L/Y57F/L58I/D59E
Variant IV	F49I/I50L/Y57F/L58I/D59E/G60E

Table 3-2: Divalent ion-binding properties data for rat β-parvalbumin, the variants and CPV3 from isothermal titration calorimetry.

VarI is the abbreviation for the 49/50 mutant; varII denotes 49/50/57/58; varIII corresponds to 49/50/57/58/59; and varIV represents 49/50/57/58/59.

Microscopic binding constants are shown with uncertainties (68% confidence intervals) parentheses. [a]Values are from Henzl et al. (2004). [b]Values are from Henzl and Agah (2006).

Divalent Ion Binding Properties

	Ca^{2+} values				Mg^{2+} values			
protein	k_1 M^{-1}	H_1 kcal/mol	k_2 M^{-1}	H_2 kcal/mol	k_{1M} M^{-1}	H_{1M} kcal/mol	k_{2M} M^{-1}	H_{2M} kcal/mol
β-PV[a]	2.30×10^7	-4.10	1.52×10^6	-3.46	9.23×10^3	3.01	1.68×10^2	4.16
	(2.05, 2.56)	(-4.16, -4.06)	1.38, 1.70)	(-3.52, -3.41)	(8.93, 9.66)	(2.97, 3.05)	(1.58, 1.79)	(4.00, 4.32)
varI	3.25×10^7	-3.53	2.32×10^6	-3.46	1.35×10^4	4.23	1.46×10^2	5.50
	(2.57, 3.80)	(-3.70, -3.31)	(1.90, 2.92)	(-3.42, -3.01)	(1.17, 1.57)	(3.98, 4.53)	(1.20, 1.66)	(5.00, 6.16)
varII	4.29×10^7	-3.78	1.5×10^6	-3.20	1.79×10^4	3.39	3.34×10^2	4.23
	(3.73, 4.68)	(-3.89, -3.66)	(1.31,1.60)	(-3.28, -3.48)	(1.65, 1.95)	(3.29, 3.52)	(2.80, 3.74)	(4.04, 4.47)
varIII	4.65×10^7	-4.92	1.70×10^6	0.16	1.92×10^4	2.50	5.09×10^2	5.34
	(4.42, 4.89)	(-5.02, -4.82)	1.64, 1.77)	(0.12, 0.19)	(1.82, 2.05)	(2.38, 2.57)	(4.68, 5.44)	(5.13, 5.56)
varIV	3.86×10^7	-3.99	2.44×10^6	2.59	1.72×10^4	3.26	5.11×10^2	5.87
	(3.46, 4.45)	(-4.24, -3.84)	(2.28, 2.88)	(2.43, 2.74)	(1.53, 1.96)	(2.91, 3.55)	(4.58, 5.71)	(5.31, 6.19)
CPV3[b]	4.50×10^7	-5.46	2.43×10^7	-0.13	4.98×10^4	1.53	2.12×10^2	1.62
	(4.31, 4.96)	(-5.68, -5.30)	(2.36, 2.66)	(-0.21, -0.04)	(4.74, 5.79)	(1.31, 1.62)	(1.94, 2.38)	(1.30, 1.76)

Table 3-3: Divalent ion-binding energetics data for rat β-parvalbumin, the variants, and CPV3 from isothermal titration calorimetry.

[a]Energies are expressed in kcal/mol. All binding data were collected in Hepes-buffered saline at pH 7.4 at 25 ˚C. [b]Equal to $-RT \ln k_1 k_2$, where R is the gas constant, T is the absolute temperature, and k_1 and k_2 are the microscopic binding constants for the first and second binding events respectively. [c]Equal to $\Delta G - \Delta H$.

Divalent Ion-Binding Energetics[a]						
	Ca^{2+} binding			Mg^{2+} binding		
Protein	ΔG^b	ΔH	$-T\Delta S$	ΔG^b	ΔH	$-T\Delta S^c$
		EF Site				
Rat β-PV	-10.04	-4.10	-5.94	-5.41	3.01	-8.42
49/50	-10.24	-3.53	-6.71	-5.63	4.23	-9.86
49/50/57/58	-10.41	-3.78	-6.63	-5.80	3.39	-9.19
49/50/57/58/59	-10.45	-4.92	-5.53	-5.84	2.50	-8.34
49/50/57/58/59/60	-10.34	-3.99	-6.35	-5.78	3.26	-9.04
CPV3	-10.43	-5.46	-4.97	-6.40	1.53	-7.93
		CD Site				
Rat β-PV	-8.43	-3.46	-4.97	-3.03	4.16	-7.19
49/50	-8.67	-3.20	-5.47	-2.94	5.50	-8.44
49/50/57/58	-8.42	-3.38	-5.04	-3.44	4.23	-8.48
49/50/57/58/59	-8.49	0.16	-8.65	-3.69	5.34	-9.03
49/50/57/58/59/60	-8.71	2.59	-11.3	-3.69	5.87	-9.56
CPV3	-10.07	-0.13	-9.94	-5.90	1.62	-7.52
		Overall				
Rat β-PV	-18.47	-7.56	-10.91	-8.44	7.17	-15.61
49/50	-18.91	-6.73	-12.18	-8.57	9.73	-18.3
49/50/57/58	-18.83	-7.16	-11.67	-9.24	7.62	-17.67
49/50/57/58/59	-18.95	-4.76	-14.19	-9.53	7.84	-17.37
49/50/57/58/59/60	-19.05	-1.40	-17.65	-9.47	9.13	-18.60
CPV3	-20.50	-5.59	-14.91	-12.36	3.15	-15.45

Table 3-4: Differential scanning calorimetry data on Ca^{2+} free rat β-PV and the variant proteins.

All experiments performed in 150 mM NaCl, 10mM NaEDTA, 10 mM NaPi, pH 7.4. Temperatures are reported in ˚Celsius and energies in kcal/mol^{-1}, and ΔC_p in kcal mol^{-1} and K^{-1}. [a]Apparent changes in conformational stability at 49.3 ºC of the wild-type T_m, calculated with eq 4-6, using the ΔC_p values determined by DSC. Apparent changes in conformational stability at 25 ºC, calculated with the ΔC_p estimates from DSC.

Protein	T_m	$\Delta\Delta T_m$	ΔH_{cal}	ΔH_{vH}	ΔC_p	$\Delta\Delta G_{conf}$[a]	$\Delta\Delta G_{conf}$[b]
wt rat β-PV	49.3 (49.2, 49.4)		72.9 (72.5, 73.1)	67.9 (67.7, 68.2)	1.60 (1.57, 1.63)		
VarI	52.7 (52.6, 52.8)	3.4	86.6 (86.3, 86.9)	69.9 (69.6, 70.1)	1.76 (1.74, 1.80)	0.69	0.20
VarII	51.2 (51.0, 51.3)	1.9	87.0 (86.7, 87.3)	66.0 (65.8, 66.2)	1.98 (1.95, 2.00)	0.37	-0.43
VarIII	51.6 (51.4, 51.7)	2.3	86.7 (86.3, 87.0)	68.3 (68.0, 68.5)	1.74 (1.72, 1.77)	0.47	0.04
VarIV	51.2 (51.1, 51.4)	1.9	86.5 (86.2, 86.8)	72.2 (72.1, 72.3)	1.70 (1.69, 1.71)	0.53	0.37

Figure 3-1: Divalent ion-binding behavior of β49/50 (VarI).

Least-squares analysis of integrated ITC data. The solid lines through the data points represent the optimal least-squares fit to the composite dataset. The residuals for each experiment, normalized to the largest signal in the titration and offset for clarity, are displayed in the lower panels.

(A). 1.0 mM Ca^{2+} vs. 63 μM β49/50 (□); 1.0 mM Ca^{2+} vs 65.7 μM β49/50, 1.0 mM NTA (○); 1.045 mM Ca^{2+} vs 65.7 μM β49/50, 3.0 mM NTA (△).

(B). 1.84 mM Mg^{2+} vs 63 μM β49/50 (□); 1.84 mM Mg2+ vs 63 μM β49/50, 100 μM EDTA (○).

(C). 1.0 mM Ca^{2+} vs 65.7 μM β49/50, 1.0mM Mg^{2+} (□); 1.0 mM Ca^{2+} vs 65.7 μM β49/50, 5 mM Mg^{2+} (○); 1.0 mM Ca^{2+} vs 63 μM β49/50, 10 mM Mg^{2+} (△).

(D). 1.0 mM Ca^{2+} vs 53 μM β49/50, 60μM EDTA (□); 1.0 mM Ca^{2+} vs 49.1 μM β49/50, 60 μM EGTA (○).

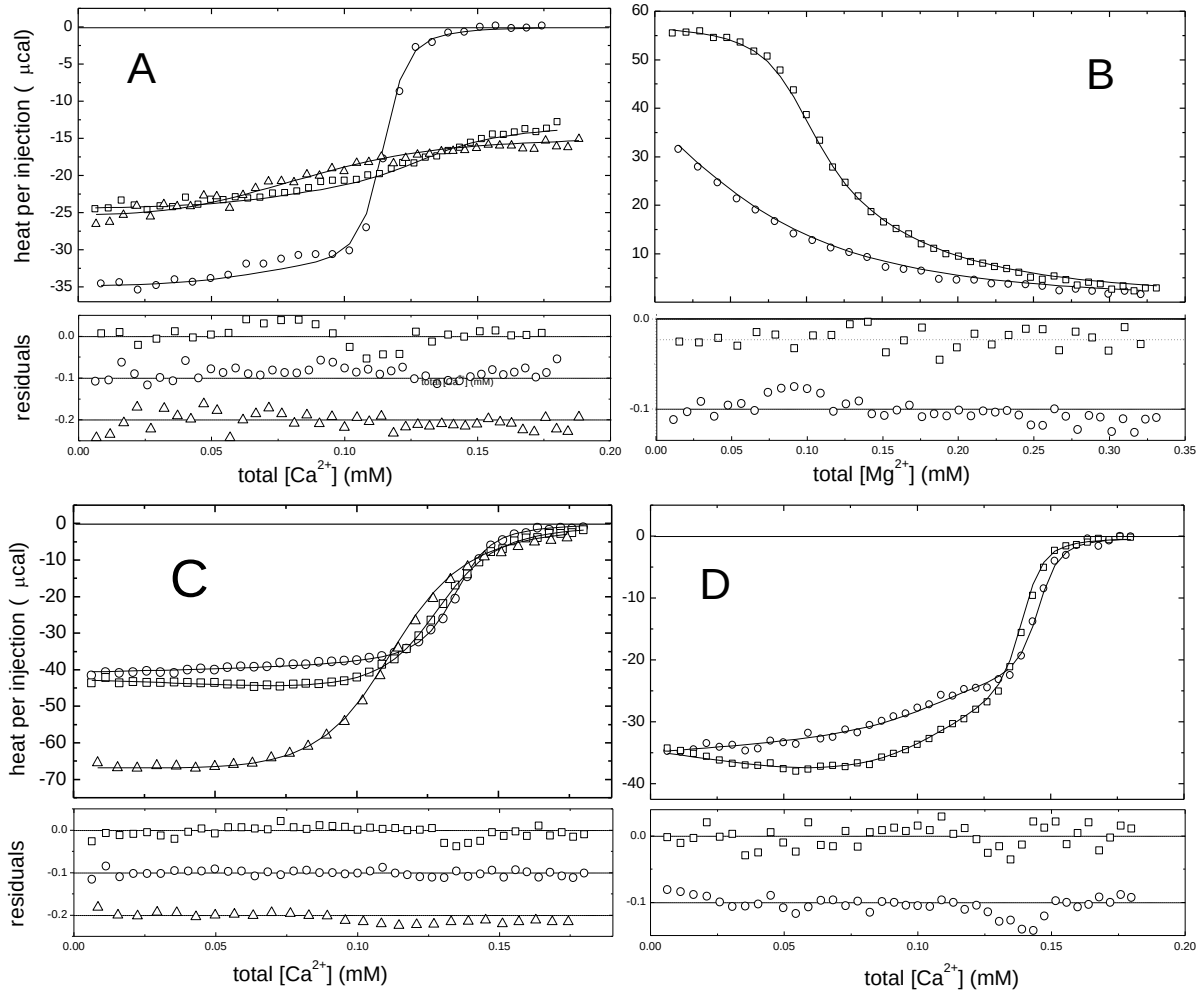
A
B
C
D
heat per injection (μcal)
residuals
total [Ca2+] (mM)
total [Mg2+] (mM)

Figure 3-2: Divalent ion-binding behavior of β49/50/57/58 (VarII).

Least-squares analysis of integrated ITC data. The solid lines through the data points represent the optimal least-squares fit to the composite dataset. The residuals for each experiment, normalized to the largest signal in the titration and offset for clarity, are displayed in the lower panels.

(A). 1.0 mM Ca^{2+} vs 65.2 μM β 49/50/57/58 (□); 1.0 mM Ca^{2+} vs 30 μM β 49/50/57/58 (○); 1.0 mM Ca^{2+} vs 65.2 μM β 49/50/57/58, 1.0 mM NTA (△); 1.0 mM Ca^{2+} vs 65.2 μM β 49/50/57/58, 3.0 mM NTA (▽).

(B). 1.84 mM Mg^{2+} vs 65.2 μM β 49/50/57/58 (□); 1.84 mM Mg^{2+} vs 65.2 μM β 49/50/57/58, 100μM EDTA (○).

(C). 1.0 mM Ca^{2+} vs 65.2 μM β 49/50/57/58, 1.0 mM Mg (□); 1.0 mM Ca^{2+} vs 65.2 μM β 49/50/57/58, 5.0 mM Mg^{2+} (○); 1.0 mM Ca^{2+} vs 65.2 μM β 49/50/57/58, 15 mM Mg (△).

(D). 1.0 mM Ca^{2+} vs 65.2 μM β 49/50/57/58, 60μM EDTA (□); 1.0 mM Ca^{2+} vs 65.2 μM β 49/50/57/58, 60μM EGTA (○).

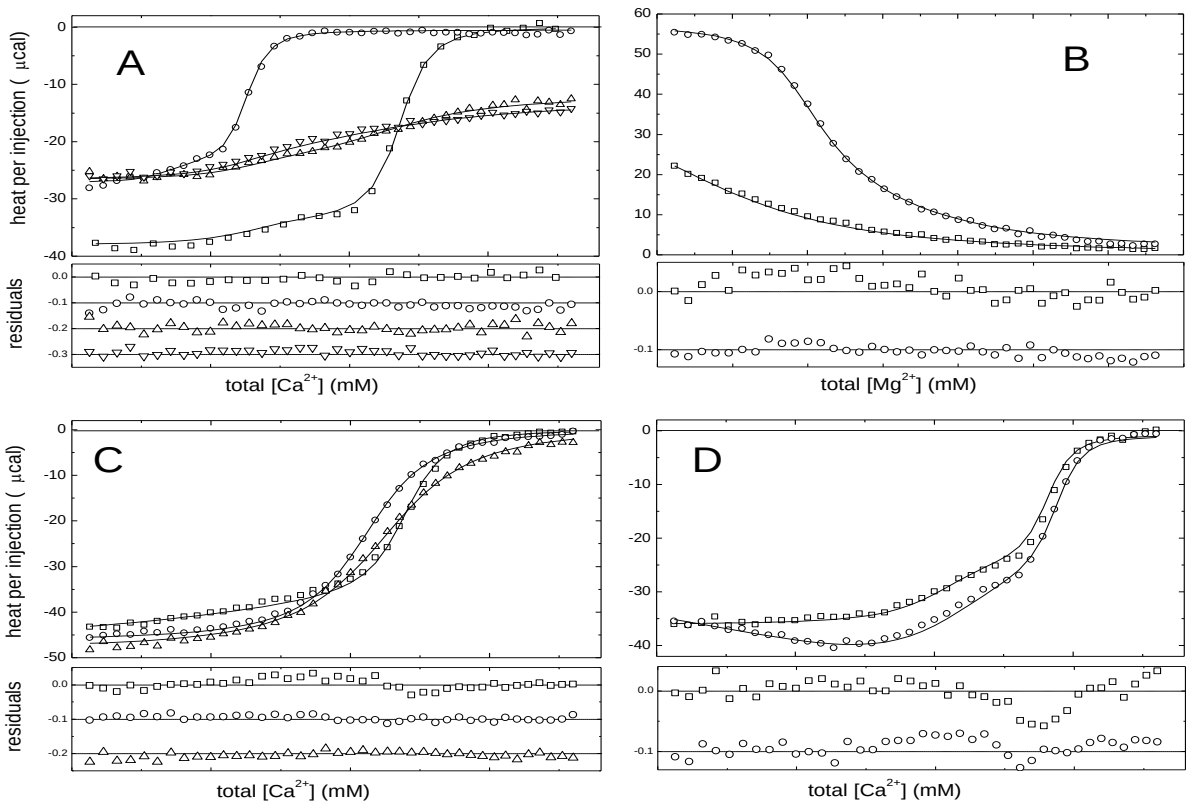
A
B
C
D
heat per injection (μcal)
residuals
total [Ca2+] (mM)
total [Mg2+] (mM)

Figure 3-3: Divalent ion-binding behavior of β49/50/57/58/59 (VarIII).

Least-squares analysis of integrated ITC data. The solid lines through the data points represent the optimal least-squares fit to the composite dataset. The residuals for each experiment, normalized to the largest signal in the titration and offset for clarity, are displayed in the lower panels.

(A) 1.0 mM Ca^{2+} vs 67 μM protein (○); 1.0 mM Ca^{2+} vs 63 μM protein and 1.0 mM NTA (□); 1.0 mM Ca^{2+} vs 66 μM protein and 0.5 mM NTA (△).

(B) 1.8 mM Mg^{2+} vs 69 μM protein (○); 1.8 mM Mg^{2+} vs 69 μM protein and 100 μM EDTA (□).

(C) 1.0 mM Ca^{2+} vs 69 μM protein and 1.0 mM Mg^{2+} (○); 1.0 mM Ca^{2+} vs 69 μM protein and 5.0 mM Mg^{2+} (□); 1.0 mM Ca^{2+} vs 65 μM protein and 10.0 mM Mg^{2+} (△).

(D) 1.0 mM Ca^{2+} vs 69 μM protein and 60 μM EDTA (○); 1.0 mM Ca^{2+} vs 64 μM protein and 60 μM EGTA (□);1.0 mM Ca^{2+} vs 60 μM protein and 60 μM EGTA (△).

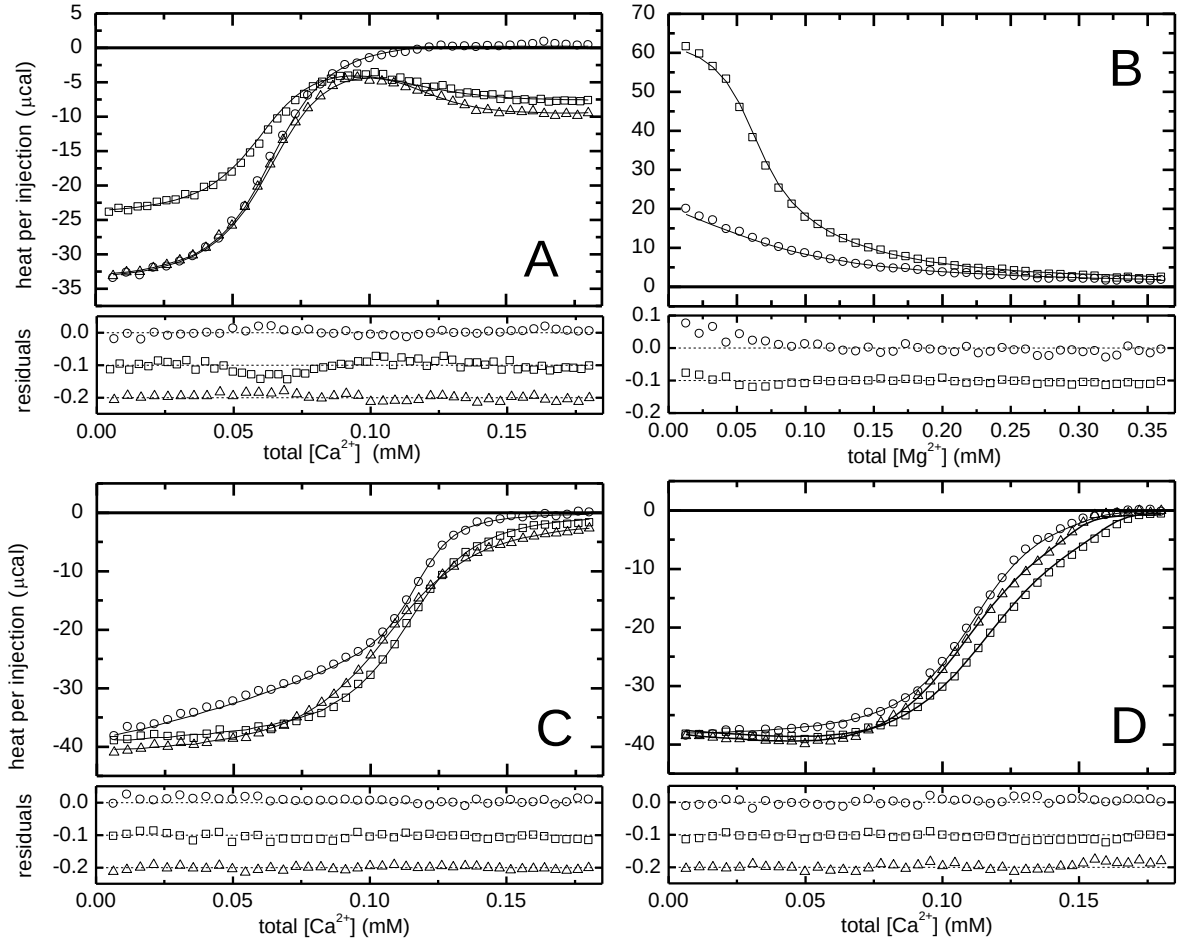
A
B
C
D
heat per injection (μcal)
residuals
total [Ca2+] (mM)
total [Mg2+] (mM)

Figure 3-4: Divalent ion-binding behavior of β49/50/57/58/59/60 (VarIV).

Least-squares analysis of integrated ITC data. The solid lines through the data points represent the optimal least-squares fit to the composite dataset. The residuals for each experiment, normalized to the largest signal in the titration and offset for clarity, are displayed in the lower panels.

(A) 1.027 mM Ca^{2+} vs 60 μM β 49/50/57/58/59/60 (□); 1.027 mM Ca^{2+} vs 30 μM β 49/50/57/58/59/60 (○); 1.027 mM Ca^{2+} vs 60 um β 49/50/57/58/59/60, 1.0 mM NTA (△).

(B) 1.84 mM Mg^{2+} vs 60 μM β 49/50/57/58/59/60 (□); 1.84 mM Mg2+ vs 63 μM β 49/50/57/58/59/60, 100 μM EDTA (○).

(C) 1.027 mM Ca^{2+} vs 60 μM β 49/50/57/58/59/60, 1.0mM Mg^{2+} (□): 1.027 mM Ca^{2+} vs 60 μM β 49/50/57/58/59/60, 5 mM Mg^{2+} (○); 1.027 mM Ca^{2+} vs 60 μM β 49/50/57/58/59/60, 10 mM Mg^{2+} (△).

(D) 1.0 mM Ca^{2+} vs 53 μM β 49/50/57/58/59/60, 60μM EDTA (□); 1.0 mM Ca^{2+} vs 49.1 μM β 49/50/57/58/59/60, 60 μM EGTA (○).

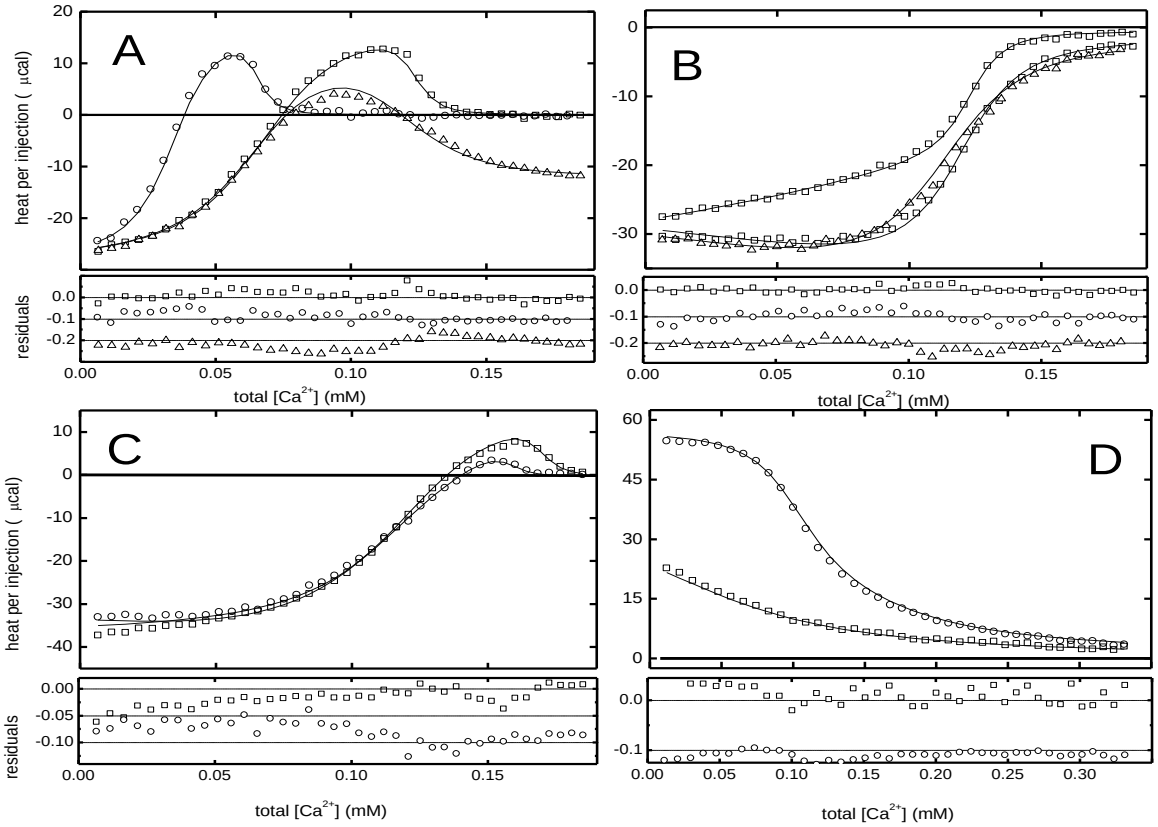
A
B
C
D
heat per injection (μcal)
residuals
total [Ca2+] (mM)

Figure 3-5: Molar heat capacity data of Ca^{2+} free rat β-PV and the variant proteins. Excess molar heat capacity is displayed as a function of temperature for wild-type β-PV (no symbol), β 49/50 (□), β 49/50/57/58 (□), β 49/50/57/58/59 (△), β 49/50/57/58/59/60 (◇). Experiment was performed in 150 mM NaCl, 10mM NaEDTA, 10 mM NaPi, pH 7.4. Temperatures are reported in Kelvin.

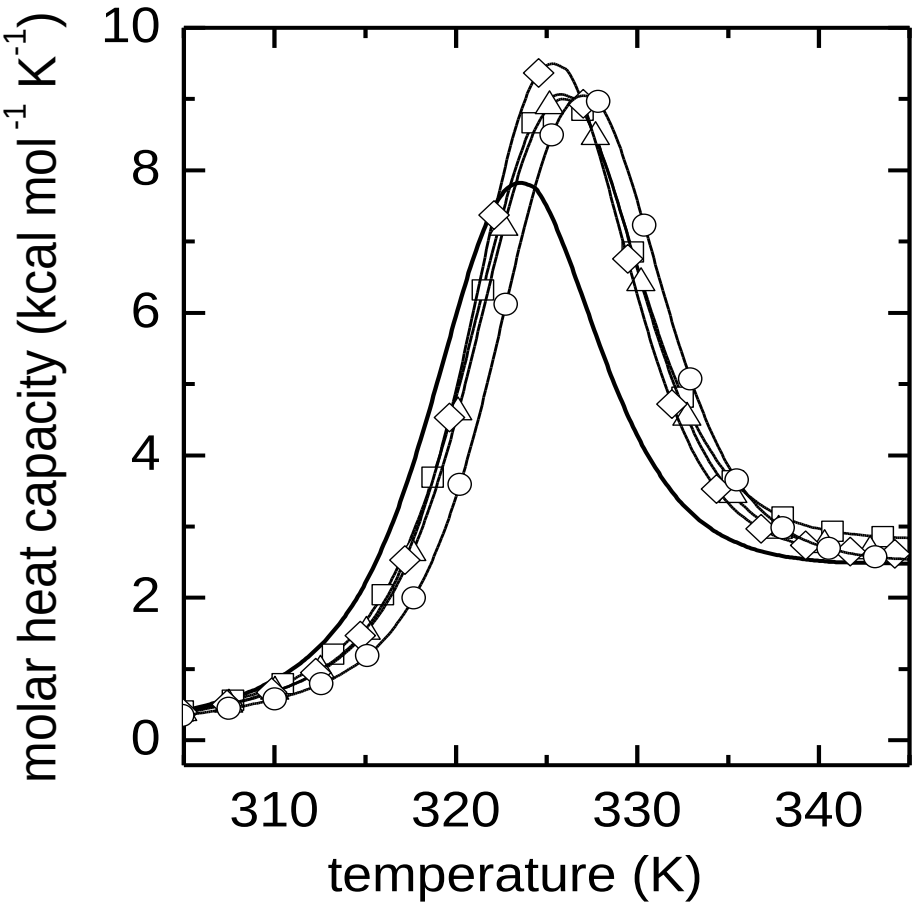
molar heat capacity (kcal mol-1 K-1)
10
8
6
4
2
0
310
320
330
340
temperature (K)

CHAPTER IV

DISCUSSION

CPV3 and Rat β-PV share 69% sequence identity (identical at 74 of the 108 residues), but exhibit highly divergent divalent ion-binding affinities in their CD sites. The CD site of rat β-PV exhibits attenuated divalent ion affinity, occupying the lower rung in the β-PV affinity spectrum. ATH resides at the higher extreme and CPV3 the middle region. Rat β and CPV3 differ in their overall binding affinity for Ca^{2+} and Mg^{2+} by 2.03 and 3.86 kcal/mol respectively (Table 3-3). These discrepancies largely reflect the disparate binding properties of their CD sites. This study addresses the question of what impact local residue nonidentities have on divalent ion binding and the overall protein stability. Specifically, residues 49, 50, 57, 58, 59, and 60 in the CD binding site of rat β-PV, were replaced with the corresponding residues from CPV3 and the effects were examined.

The sequence of the engineered CD site in the β 49/50/57/58/59/60 variant is identical to CPV3 at 27 of 30 residues. The remaining residues at 43, 45 and 69 are highly conservative. At position 43, valine replaces leucine. The presence of a terminal isopropyl group in the apolar side chain of leucine and its valine replacement is expected to cause only minor effects on protein packing. Position 45 is solvent-accessible and the substitution of glutamate with aspartate is expected to have an insignificant impact due to the replacement of one anionic side-chain for another. Lastly, at position 69, lysine replaces arginine. Both side chains couple an apolar spacer and a cationic functional group. In the X-ray structure of Ca^{2+}-bound rat β (Ahmed et al., 1993), the ε amino group

of Lys-69 is hydrogen-bonded to the side-chain amide carbonyl of Asn-52. The guanidinium group of arginine could perform a similar function in CPV3. Consequently, the behavior of variant IV offers a practical measure of the relative influence of local and remote structural determinants on the CD site divalent ion-binding character. The impact of these rat β → CPV3 mutations on apo-protein stability and divalent ion affinity is discussed below.

A. Conformational Stability

The ratio of $\Delta H_c/\Delta H_{vH}$ is often used to detect two-state behavior. Values near 1.0 indicate negligible population of intermediate states. The ratio obtained for wild-type β-PV (1.07) satisfies this criterion. However, the four variant proteins exhibit significantly higher values: 1.24 for varI, 1.32 for varII, 1.27 for varIII , and 1.20 for varVI. These elevated $\Delta H_c/\Delta H_{vH}$ ratios are largely the product of their elevated ΔH_c values ($\Delta\Delta H$ = 14 Kcal/mol). Considering the entire rat β-PV amino acid sequence, it is possible the β-PV → CPV3 mutations at positions 49, 50, 57, 59, and 60, of the CD site could diminish the cooperativity of the unfolding transition and lead to a larger population of partially folded intermediates.

Theoretically, deprotonation events could alter the apparent calorimetric enthalpy. Of the six mutations under consideration, only D59E and G60E, involve ionizable side chains. However, Glu-59 and Glu-60 will be ionized at the pH employed for the study. Moreover, carboxylates have small enthalpies of ionization. In principle, the mutations could perturb the p*K* values of adjacent residues. However, there are few candidates with the qualities to fit the requisite ionization profile, protonated in the native state,

deprotonated in the denatured state. His-107 would be a possibility if engaged in a salt bridge in the folded protein. However, the crystal structure of Ca^{2+}-bound rat β-PV reveals no anionic side chains in the immediate vicinity of the imidazole ring. Moreover the enthalpy of ionization is just 8.6 kcal/mol (Fukada and Takahashi, 1998).

Alternatively, the increased calorimetric enthalpy could involve coupled temperature-dependent binding which has been known to contribute to the apparent energetics of a process (Eftink et al., 1983; Ferrari and Lohman, 1994; and Kozlov and Lohman, 2000). Prior studies provide evidence that Ca^{2+}-free rat β binds in excess of one equivalent of Na^+. The elevated ΔH_{cal} values could possibly be as a result of monovalent Na^+ or K^+ binding.

DSC studies provide an estimate of the apparent ΔC_p. VarI housing the F49I and I50L mutations displays a significant increase in the apparent ΔC_p with respect to wildtype rat β-PV (Table 3-4). With the introduction of Y57F and L58I, the ΔC_p is raised even further. This trend is reversed in VarIII and IV following additional D59E and G60E substitutions. The ΔC_p decreases such that the value of varIV (ΔC_p = 1.70 kcal $mol^{-1}K^{-1}$) which is most similar to CPV3 is comparable to that of wild-type β-PV (ΔC_p = 1.60 kcal $mol^{-1}K^{-1}$) (Table 3-4).

At the wild-type *T*m (49.3 °C), all four variants exhibit elevated stability with $\Delta\Delta G_{conf}$ values between 0.37 kcal/mol (for varII) and 0.69 kcal/mol (for varI) (Table 3-4). Because of the apparent changes in ΔC_p, the anticipated impact of the mutations at 25 °C is variable. VarI and varIV are projected to be more stable than wild-type β-PV, exhibiting apparent changes in conformational stability of 0.20 and 0.37 kcal/mol, respectively measured at 25 °C. By contrast, varII is projected to be 0.43 kcal/mol less

stable, and the extrapolated stability of varIII is comparable to that of wild-type β-PV ($\Delta\Delta G_{conf}{}^{b}$ = 0.04 kcal/mol) (Table 3-4).

The Henzl lab has indicated that the DSC predictions show some inconsistencies with urea denaturation studies conducted at 25 °C (Henzl and Ndubuka, 2007). Their results indicate that 49/50/57/58 exhibits slightly greater stability than wild-type β-PV. The study also indicated lower ΔC_p values than those acquired by DSC for the variants and wild-type β-PV.

The decrease in ΔC_p values when calculated by DSC as compared to urea denaturation analysis is not unique to this set of proteins. McCrary et al. (1996) observed that Sac7d, a DNA-binding protein from *Sulfolobus acidicaldarius* also displayed such discrepancies. The higher ΔC_p value generated by urea denaturation was later traced to the impact of protonation and anion-binding events on protein folding (McCary et al., 1998). It is possible that a similar phenomenon involving monovalent ion-binding might be responsible for the behavior described herein.

The Henzl lab results are indicative of improved side-chain packing and greater efficiency in the burial of the apolar side surface upon the introduction of F49I/I50L mutations as evidenced by the increase in ΔC_p. This trend is continued with the introduction of Y57F and L58I mutations into variant I. The ΔC_p reaches its maximal value in variant II. Addition of the D59E substitution into variant II causes a reduction in ΔC_p, returning it to a value comparable to variant I (Table 3-4). The substitution of Gly-60 with glutamate in variant IV has little additional impact on ΔC_p in comparison to variant III (Henzl and Ndubuka, 2007).

B. Divalent Ion Binding.

The variants display differences in binding affinity as compared to wild-type β-PV. It should be noted that although the differences are modest, for two of the variants, the comparatively minor changes in ΔG are accompanied by much larger, but compensating changes in binding enthalpy and entropy.

VarI: F49I/I50L

The F49I/I50L mutations induce minor increases in affinity at both the CD and EF sites, which correspond to an improvement in Ca^{2+} and Mg^{2+} binding of 0.44 and 0.13 kcal/mol respectively (Table 4-3). Figure 4-3 represents a graphical illustration of the changes in affinity. Following the substitutions, the reason for enhanced binding affinity could be a result of improved side-chain packing in the apo-protein accompanied by diminished protein folding. If this were the case, the resulting binding enthalpy should be less exothermic and the conformational entropy penalty less severe. The $\Delta\Delta H$ and $-T\Delta\Delta S$ values fit this rationale (0.83 kcal/mol and -1.27 kcal/mol, respectively for Ca^{2+}; 2.56 and -2.69 kcal/mol for Mg^{2+}) (Table 4-3).

VarII: F49I/I50L/Y57F/L58I

Together, the Y57F and L58I mutations have a divergent effect on the Ca^{2+} affinity of the EF and CD sites. The EF site further improves upon the enhanced Ca^{2+} affinity displayed by varI ($\Delta\Delta G$ = -0.17 kcal/mol) (Table 4-1 and Figure 4-1), but the CD site exhibits a decrease in Ca^{2+} affinity ($\Delta\Delta G$ = 0.25 kcal/mol) (Table 4-2 and Figure 4-

2). The reduction in affinity of the CD site results in a nominal overall free energy change for Ca^{2+} binding ($\Delta\Delta G$ = 0.08 kcal/mol) (Table 4-3).

In light of the reduction in Ca^{2+} affinity of the CD site and the minimal alteration of the overall free energy change exhibited for Ca^{2+} binding, it is interesting that the strength of Mg^{2+} binding shows a respectable increase in both binding sites with respect to β 49/50 ($\Delta\Delta G$ = -0.17 kcal/mol and -0.5 kcal/mol for the EF and CD sites respectively).

DSC analysis indicates the amino acid alterations destabilize the protein. The mutations lower ΔH_{vH} by 3.9 kcal/mol (Table 3-4). The melting temperature is decreased by 1.5 °C in comparison to varI but is still greater than wild-type by 1.9 °C (Table 3-4). This reduced stability could be suggestive of inferior side-chain packing in the apoprotein. Accordingly, Ca^{2+} binding should oblige a higher degree of protein folding. The overall Ca^{2+} binding enthalpy ($\Delta\Delta H$ = -0.4 kcal/mol) and the compensatory entropic component ($-T\Delta\Delta S$ = 0.51 kcal/mol) are supportive of this explanation.

VarIII: F49I/I50L/Y57F/L58I/D59E

Glutamate is present at position 59 (-*x* position of the CD site) in every PV except the mammalian β isoform, where it is aspartate. It had been assumed that this single sequence difference was largely responsible for the attenuated divalent ion-binding behavior of rat β in comparison to other members of the β sublineage. The replacement of Asp-59 by glutamate, however, indicates that the source of reduced divalent ion affinity of the CD site resides elsewhere. A D59E substitution in wild-type rat β improves the Ca^{2+} affinity by a meager 0.1 kcal/mol (Hapak et al., 1989). Note however that the

converse mutation in rat α produces a significant impact on Ca^{2+} binding ($\Delta\Delta G$ = +1.6 kcal/mol) (Henzl et al, 2004). Evidently the ligand occupying *–x* position can shape the binding properties of the CD site, but its impact is highly context-dependent. Subsequent introduction of D59E substitution to varII produces a $\Delta\Delta G$ of -0.14 kcal/mol similar to the change of -0.1 kcal/mol seen in wild-type β.

With respect to β49/59/57/58, DSC analysis indicates that addition of the D59E mutation raises the van't Hoff enthalpy for thermal denaturation by 2.3 kcal/mol and the melting temperature by 0.4 °C (Table 3-4). The projected ΔC_p indicates a reduction of 0.24 kcal mol^{-1} K^{-1} (Table 3-4). It seems that the -0.14 kcal/mol increase in overall Ca^{2+}-affinity presumably results from a minor stabilization of the bound state ($\Delta\Delta G_{conf}{}^{b}$ = 0.04 kcal/mol) (Table 3-4).

The minor improvement in Ca^{2+}-binding free energy, which is coupled with the CD site, is accompanied by large compensating changes in binding enthalpy ($\Delta\Delta H$ = 3.54 kcal/mol) and entropy ($-T\Delta\Delta S$ = -3.61 kcal/mol) (Table 4-2) Figure (4-2) provides a graphical representation of these changes. Although the $\Delta\Delta G$ associated with the EF site is negligible, the binding enthalpy is significantly improved ($\Delta\Delta H$ = -1.14 kcal/mol) (Table 4-1).

Mg^{2+} binding displays comparable energetic characteristics to those shown by Ca^{2+}. Similar to the overall Ca^{2+} affinity signature, the CD site is a major contributor to the improved overall binding affinity (The CD site and the EF site contribute -0.25 kcal/mol and -0.04 kcal/mol respectively) (Table 3-3). Although the $\Delta\Delta G$ associated with the EF site is minute, the binding is significantly more exothermic ($\Delta\Delta H$ = -0.89

kcal/mol) (Table 3-3). Binding at the CD site is distinctly more endothermic ($\Delta\Delta H$ = 1.11 kcal/mol), but the magnitude of the change is less than that for Ca^{2+} (Table 3-3).

In Ca^{2+}-bound rat β, water serves as the proximal *–x* ligand in the CD site. The H_2O molecule forms a bridge between the Ca^{2+} and the carboxylate of Asp-59 (Ahmed et al., 1993). As previously mentioned, position 59 is occupied by glutamate in every other PV that has so far been examined. At this position, glutamate is in direct coordination with the divalent ion. The replacement of Asp-59 by glutamate should liberate a water molecule, thereby producing more favorable binding entropy. The impact created by the D59E mutation in varII closely parallels that observed in wild-type β-PV (Henzl et al., 2004). That system also displays an increase in exothermicity at the EF site and a significant decreased exothermic CD site binding event. The increased Ca^{2+} affinity at the CD site is a product of a minor reduction in its entropy.

The structural and thermodynamic relationship that exists between the two PV binding sites is manifested by the modification of the divalent ion binding at the EF site by the D59E mutation in the CD binding loop. In the bound form, the two Ca^{2+}-binding loops are connected by a short segment of antiparallel beta structure, involving residues 57 and 58 in the CD loop and residues 96 and 97 in the EF loop. Although the extent to which this structural property is present in the apo-protein is unknown, the proximity of the two loops in this region increases the probability that a perturbation of the CD site main-chain dynamics would be transmitted to the EF site.

VarIV: F49I/I50L/Y57F/L58I/D59E/G60E

The addition of the G60E mutation to varIII produces results similar to those produced upon the introduction of D59E to varII. Ca^{2+} affinity is slightly improved ($\Delta\Delta G$ = -0.11 kcal/mol), the binding properties of both sites is affected; $\Delta\Delta G$ = 0.11 kcal/mol and -0.22 kcal/mol for the EF and CD sites respectively (Table 3-3). However, they differ in that G60E induces a minor reduction ($\Delta\Delta G$ = 0.06 kcal/mol) in overall Mg^{2+} affinity (Table 3-3). Furthermore, the $\Delta\Delta G$ is accompanied by compensating Ca^{2+}-binding enthalpic and entropic values ($\Delta\Delta H$ = 0.93 and 2.43 kcal/mol for the EF and CD sites respectively; $-T\Delta\Delta S$ = 0.82 and -2.65 kcal/mol correspondingly) (Table 3-3). Recall that varI displayed a similar energetic signature, positive $\Delta\Delta H$ and negative $-T\Delta\Delta S$. With its increase in denaturational ΔC_p, these changes to wild-type β-PV were interpreted to indicate improved side-chain packing in the apoprotein. However, the G60E mutation is not accompanied by a similar increase in denaturational ΔC_p, and the introduction of an additional anionic residue into the anionic CD binding loop is not expected to induce more efficient folding.

The thermodynamic impact of G60E could imply an alteration in conformational entropy. The glutamate substitution at position 60 should restrict motion in the bound state producing a more favorable $-T\Delta\Delta S$ for Ca^{2+}-binding. It is, however, unlikely that the $-T\Delta\Delta S$ value of -3.44 kcal/mol (Table 4-3) observed for G60E could solely be attributed to a reduction in main-chain conformational entropy.

Mg^{2+} binding thermodynamic properties are less affected by the G60E mutation ($\Delta\Delta H$ = 1.29 kcal/mol, $-T\Delta\Delta S$ = -1.23 kcal/mol) (Table 4-3). Spectroscopic and structural studies performed by Blancuzzi et al. (1993), and Declercq et al. (1991) respectively indicate that Mg^{2+} binding is accompanied by a smaller conformational

change compared to Ca^{2+} binding. The reduced values for $\Delta\Delta H$ and $-T\Delta\Delta S$ might reflect ionic interactions involving E60 in the apo-protein that are preserved upon Mg^{2+} binding.

C. Conclusions

Rat β-parvalbumin and chicken parvalbumin 3 are identical at 74 of 108 residues, yet rat β exhibits lower Ca^{2+} and Mg^{2+} affinities. Incorporating six site-specific mutations, the CD site in rat β (residues 41- 70) is rendered identical to that of CPV3 at 27 of the 30 residues. Rat β-PV is the only parvalbumin studied to date that possesses aspartate at position 59; all others carry Glu-59. This discrepancy had previously been thought to be responsible for its attenuated divalent ion affinity at the CD site. However, even with the D59E substitution the Ca^{2+} and Mg^{2+} affinities of varIV remain, respectively, 1.5 and 2.9 kcal/mol less favorable than that of CPV3. The ΔH following Ca^{2+} binding to the CD site is 0.13 kcal/mol. VarIV displays a marked difference in a value of 2.56 kcal/mol.

The three remaining nonidentities in the CD site reflect highly conservative substitutions – valine vs. leucine at position 43, aspartate vs. glutamate at position 45, and lysine vs. arginine at position 69. Thus, the results of this study strongly indicate that the residues responsible for the unusual divalent ion-binding signature of the mammalian β-parvalbumin isoform reside beyond the borders of the CD site EF-hand motif.

Table 4-1: EF site divalent ion-binding energetics data for wild-type rat β-parvalbumin, and the variants.

[a]Energies are expressed in kcal/mol. All binding data were collected in Hepes-buffered saline at pH 7.4 at 25 ˚C. [b]Equal to $-RT \ln k_1k_2$, where R is the gas constant, T is the absolute temperature, and k_1 and k_2 are the microscopic binding constants for the first and second binding events respectively. [c]Equal to $\Delta G - \Delta H$.

	ΔG_{ca}	ΔH_{Ca}	$-T\Delta S_{Ca}$	ΔG_{Mg}	ΔH_{Mg}	$-T\Delta S_{Mg}$
Rat β –PV	-10.04	-4.1	-5.95	-5.41	3.01	-8.42
variant1	-10.24	-3.53	-6.71	-5.63	4.23	-9.86
variant2	-10.41	-3.78	-6.63	-5.8	3.39	-9.19
variant3	-10.45	-4.92	-5.53	-5.84	2.5	-8.34
variant4	-10.34	-3.99	-6.35	-5.78	3.26	-9.04
CPV3	-10.43	-5.46	-4.97	-6.4	1.53	-7.93

Figure 4-1: Graphical representation of EF site divalent ion-binding energetics data for wild-type rat β-parvalbumin, and the variants.

.

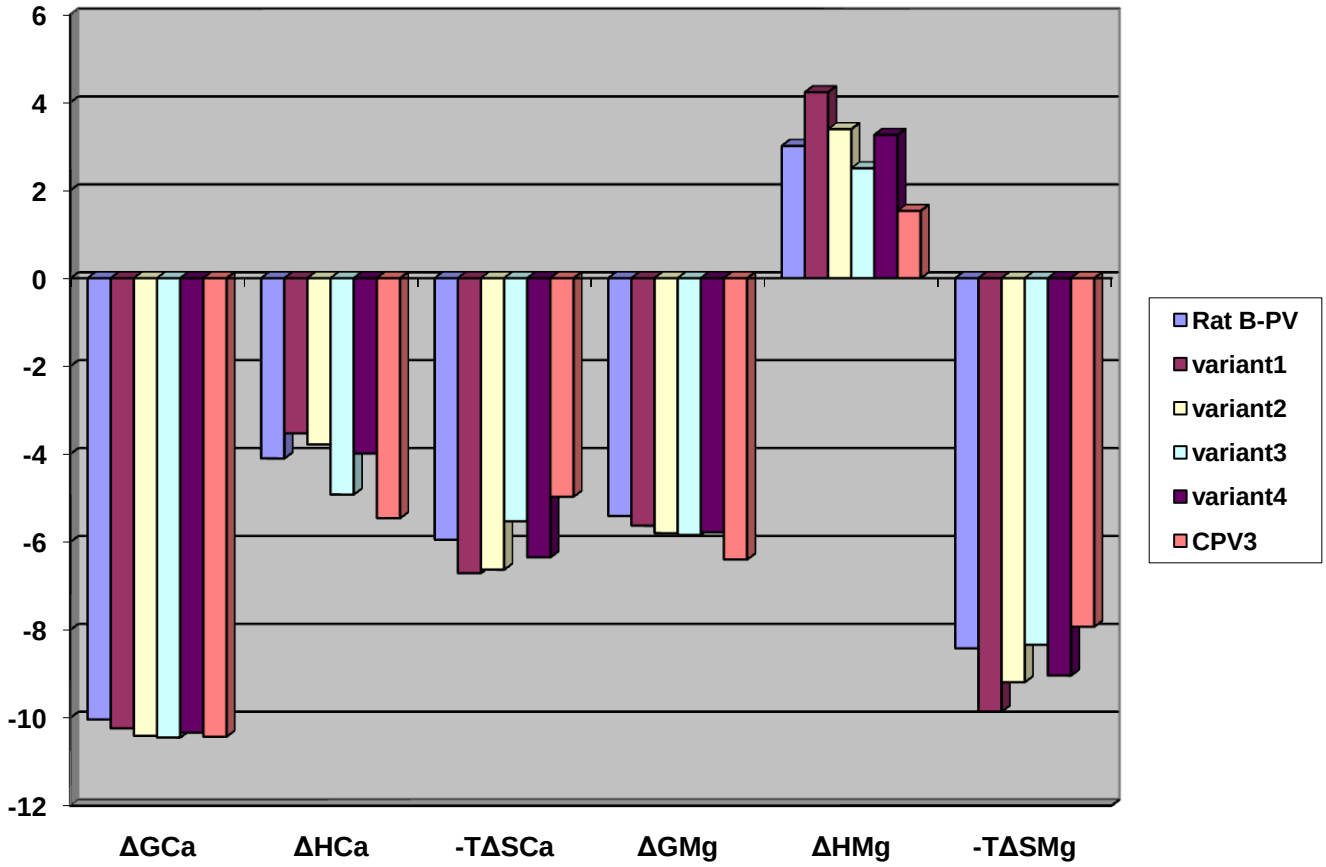
6
4
2
0
-2
-4
-6
-8
-10
-12
ΔGCa
ΔHCa
-TΔSCa
ΔGMg
ΔHMg
-TΔSMg
Rat B-PV
variant1
variant2
variant3
variant4
CPV3

Table 4-2: CD site divalent ion-binding energetics data for wild-type rat β-parvalbumin, and the variants.

[a]Energies are expressed in kcal/mol. All binding data were collected in Hepes-buffered saline at pH 7.4 at 25 ˚C. [b]Equal to $-RT \ln k_1k_2$, where R is the gas constant, T is the absolute temperature, and k_1 and k_2 are the microscopic binding constants for the first and second binding events respectively. [c]Equal to $\Delta G - \Delta H$.

	ΔG	ΔH	-TΔS	ΔG	ΔH	-TΔS
β–PV	-8.43	-4.46	-4.97	-3.03	4.16	-7.19
Variant1	-8.67	-3.2	-5.47	-2.94	5.5	-8.44
Variant2	-8.42	-3.38	-5.04	-3.44	4.23	-8.48
Variant3	-8.49	0.16	-8.65	-3.69	5.34	-9.03
Variant4	-8.71	2.59	-11.3	-3.69	5.87	-9.56
CPV3	-10.07	-0.13	-9.94	-5.9	1.62	-7.52

Figure 4-2: Graphical representation of CD site divalent ion-binding energetics data for wild-type rat β-parvalbumin, and the variants.

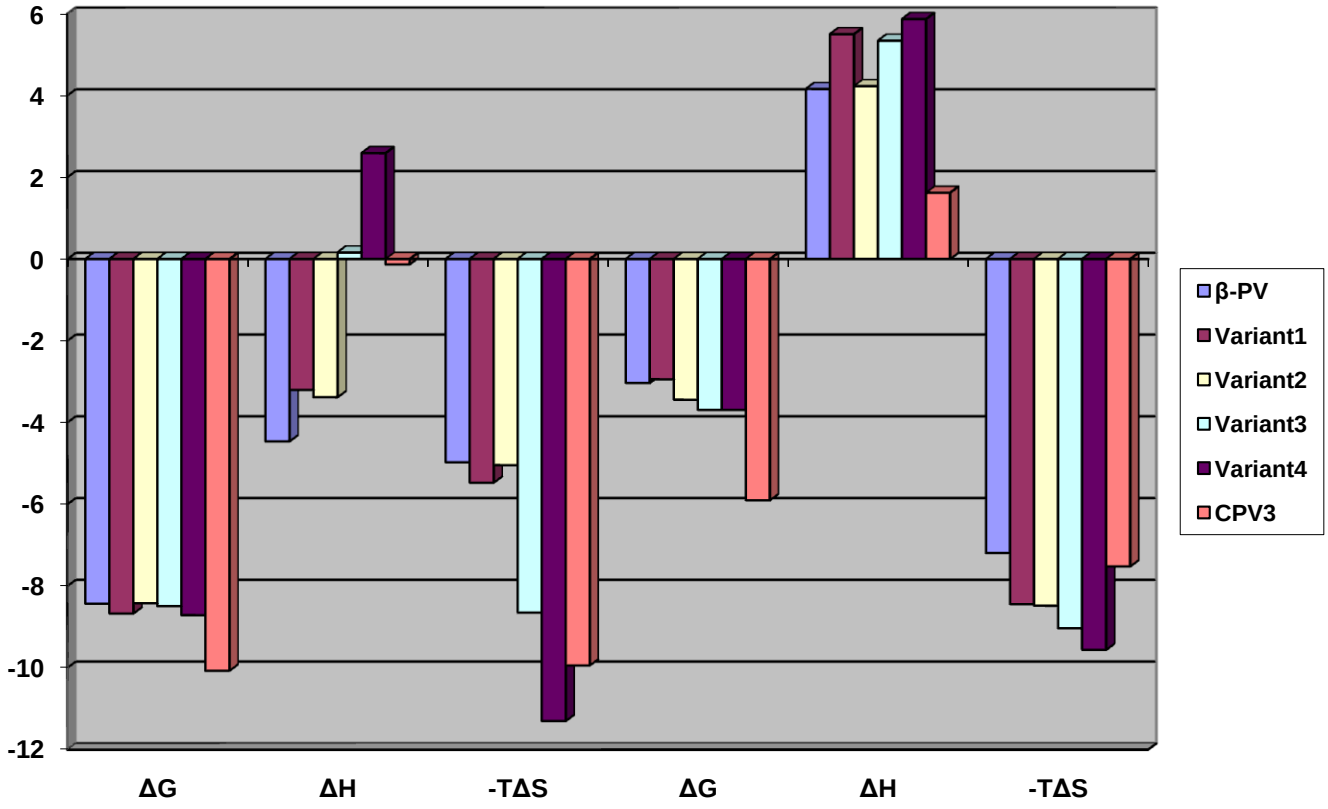
6
4
2
0
-2
-4
-6
-8
-10
-12
ΔG
ΔH
-TΔS
ΔG
ΔH
-TΔS
β-PV
Variant1
Variant2
Variant3
Variant4
CPV3

Table 4-3: Overall divalent ion-binding energetics data for wild-type rat β-parvalbumin, and the variants.

[a]Energies are expressed in kcal/mol. All binding data were collected in Hepes-buffered saline at pH 7.4 at 25 ˚C. [b]Equal to $-RT \ln k_1k_2$, where R is the gas constant, T is the absolute temperature, and k_1 and k_2 are the microscopic binding constants for the first and second binding events respectively. [c]Equal to $\Delta G - \Delta H$.

	ΔG_{Ca}	ΔH_{Ca}	$-T\Delta S_{Ca}$	ΔG_{Mg}	ΔH	$-T\Delta S_{Mg}$
Rat β –PV	-18.47	-7.56	-10.91	-8.44	7.17	-15.61
variant	-18.91	-6.73	-12.18	-8.57	9.73	-18.3
variant2	-18.83	7.16	-11.67	-9.24	7.62	-17.67
variant3	-18.95	-4.76	-14.19	-9.53	7.84	-17.37
variant4	-19.05	-1.4	-17.65	-9.47	9.13	-18.6
CPV3	-20.05	-5.59	-14.91	-12.36	3.15	-15.45

Figure 4-3: Graphical representation of overall divalent ion-binding energetics data for wild-type rat β-parvalbumin, and the variants.

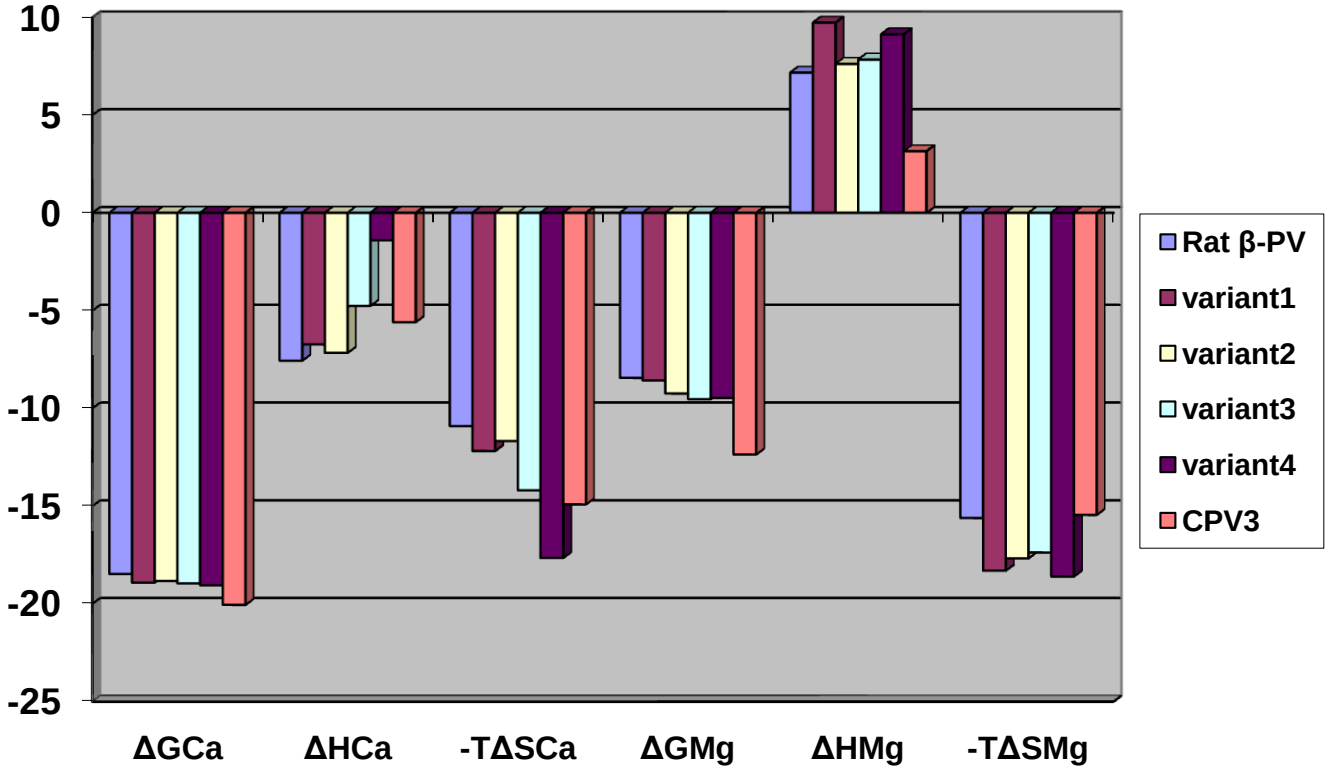
10
5
0
-5
-10
-15
-20
-25
ΔGCa
ΔHCa
-TΔSCa
ΔGMg
ΔHMg
-TΔSMg
Rat β-PV
variant1
variant2
variant3
variant4
CPV3

REFERENCES

1. Ahmed, F. R., Rose, D. R., Evans S. V., Pippy, M. E., and To, R. (1993) Refinement of recombinant oncomodulin at 1.30 Å resolution. *J. Mol. Biol. 230,* 1216—1224.

2. Berridge, M.J. (1993) Inositol trisphosphate and calcium signaling. *Nature 361*, 314-325.

3. Blancuzzi, Y., Padilla, A., Parello, J., and Cave, A. (1993) Symmetrical rearrangement of the cation-binding sites of parvalbumin upon Ca^{2+}/Mg^{2+} exchange. A study by ^{1}H 2D NMR. *Biochemistry 32,* 1302-1309.

4. Blum, J.K., and Berchtold, M.W. (1994). Calmodulin like effects of oncomodulin on cell proliferation. *J. Cell. Physiol. 160(3),* 655-662.

5. Brewer, J.M., Wunderlich, J.K., Kim, D.H., Carr, M.Y., Beach, G.G., Ragland, W.L. (1989) Avian thymic hormone (ATH) is a parvalbumin. *Biochem Biophys Res Commun*. *160,* 1155-1161.

6. Briggs, N. (1975) Identification of the soluble relaxing factor as a parvalbumin. *Fed Proc. 34,* 540.

7. Caillard, O., Moreno, H., Schwaller, B., Llano, I., Celio, M. R., and Marty, A. (2000) Role of the calcium-binding protein parvalbumin in short-term synaptic plasticity. *Proc. Natl. Acad. Sci. USA 97,* 13372-13377.

8. Clayshulte, T.M., Taylor, D.F., Henzl, M.T. (1990) Reactivity of cysteine 18 in oncomodulin. *J Biol Chem 265*, 1800-1805.

9. Cox, J.A., Milos, M., and MacManus, J.P. (1990) Calcium- and magnesium-binding properties of oncomodulin. *J. Biol. Chem. 265,* 6633-6637.

10. Celio, M.R., Pauls, T.L., and Schwaller, B. (1996) Introduction to EF-hand calcium-binding proteins. In "Guidebook to the calcium-binding proteins." Edited by Celio, M.R., Oxford Univ. Press. Pp 15-20.

11. Declercq, J.P., Tinant, B., Parello, J., and Rambaud, J. (1991) Ionic interactions with parvalbumins. Crystal structure determination of pike 4.10 parvalbumin in four different ionic environments, *J. Mol. Biol. 220*, 1017-1039.

12. Durkin, J.P., Brewer, L.M., and MacManus, J.P. (1983) Occurrence of the tumor-specific calcium-binding protein oncomodulin in virally transformed normal rat kidney cells. *Cancer Res. 43(11),* 5390-5394.

13. Eftink, M. R., Anusien, A. C., and Biltonen, R. L. (1983) Enthalpy-entropy compensation and heat capacity changes for protein-ligand interactions: general thermodynamic models and data for the binding of nucleotides to ribonuclease A. *Biochemistry 22,* 3884-3896.

14. Falke, J.J., Darke, S.K., Hazard, A.L., and Peersen, O.B. (1994) Molecular tuning of ion binding to calcium signaling proteins. *Quart. Rev. Biophys. 27(3),* 219-290

15. Ferrari M. E., and Lohman, T.M. (1994) Apparent heat capacity change accompanying a nonspecific protein-DNA interaction, *Biochemistry 33,* 12896-12910.

16. Fohr, U.G., Weber, B.R., Muntener, M., Staudenmann, W., Hughes, G.J., Frutiger, S., Banville, D., Schafer, B.W., and Heizmann, C.W. (1993) Human alpha and beta parvalbumins. Structure and tissue-specific expression. *Eur. J. Biochem. 215*, 719-727.

17. Fukada, H., and Takahashi, K. (1998) Enthalpy and heat capacity changes for the proton dissociation of various buffer components in 0.1 M potassium chloride. *Proteins 33,* 159-166.

18. Furter, C.S., Heizmann, C.W., Berchtold, M.W., (1989) Isolation and analysis of a rat genomic clone containing a long terminal repeat with high similarity to the oncomodulin mRNA leader sequence. *J. Biol. Chem. 264*, 18276-18279.

19. Goodman, M., and Pechere, J.F. (1977) The evolution of muscular parvalbumins investigated by the maximum parsimony method. *J. Mol. Evol. 9,* 131-158.

20. Haiech, J., Derancourt, J., Pechere, J.F., and Demaille, J.G. (1979) Magnesium and calcium-binding to parvalbumins: Evidence for differences between parvalbumins and an explanation of their relaxing functions. *Biochem. 18(3),* 2752-2758.

21. Gerday, C., and Gillis, J.M. (1976) The possible role of parvalbumins in the control of contraction. *J. Physiol. 258(2),* 96-97.

22. Gillis, J.M., Thomason, D., LeFever, J., and Kretsinger, R.H. (1984) formation of calcium-parvalbumin complex during contraction. A source of unexplained heat? *Adv. In Exper. Med. And Bio. 170,* 573-579.

23. Haiech, J., Klee, C.B., and Demaille, J.G. (1981) Effects of cations on affinity of calmodulin for calcium: Ordered binding of calcium ions allows the specific activation of calmodulin-stimulated enzymes. *Biochem. 20(13):* 3890-3897.

24. Hapak, R.C., Lammers, P.J., Palmisano, W.A., Birnbaum, E.R., Henzl, M.T. (1989) Site-specific substitution of glutamate for aspartate at position 59 of rat oncomodulin. *J. Biol. Chem. 264*, 18751-18760.

25. Hapak, R.C., Stanley, C.M., Henzl, M.T. (1996) Intrathymic distribution of the two avian thymic parvalbumins. *Exp. Cell. Res. 222*, 234-245.

26. Heizmann, C.W., and Strehler, E.E. (1979) Chicken parvalbumin. Comparison with parvalbumin-like protein and three other components (Mr = 8,000 to 13,000). *J. Biol. Chem. 254(10),* 4296-4303.

27. Heller, S., Bell, A.M., Denis, C.S., Choe, Y., Hudspeth, A.J. (2002) Parvalbumin 3 is an abundant Ca^{2+} buffer in hair cells. *J. Assoc. Re.s Otolaryngol. 3*, 488-498.

28. Henzl, M.T., and Agah, S. (2006) Divalent ion-binding properties of the two avian β-parvalbumins. *Proteins 62,* 270-278.

29. Henzl M.T., Agah S, Larson J.D. (2004) Rat α- and β-parvalbumins: comparison of their pentacarboxylate and site-interconversion variants. *Biochemistry 43*, 9307-9319.

30. Henzl, M.T., and Graham, J.S. (1999) Conformational stabilities of the rat α- and β-parvalbumins, *FEBS Lett. 442*, 241-245.

31. Henzl, M.T., Hapak, R.C., and Likos, J.J. (1998) Interconversion of the ligand arrays in the CD and EF sites of oncomodulin. Influence on Ca^{2+}-binding affinity, *Biochemistry 37,* 9101-9111.

32. Henzl, T. M., and Ndubuka, K. (2007) Low-affinity signature of the Rat β-parvalbumin CD site. Evidence for remote determinants, *Biochemistry 45*, 23—35.

33. Henzl, M. T., Shibasaki, O., Comegys, T. H., Thalmann, I., and Thalmann, R. (1997) Oncomodulin is Abundant in the Organ of Corti. *Hear. Res. 106*, 105-111.

34. Henzl, M.T., Agah, S., and Larson, J.D. (2003) Characterization of the metal ion-binding domains from rat α- and β-parvalbumins. *Biochemistry 42*, 3594 – 3607.

35. Henzl, M.T., Larson, J.D., and Agah, S. (2003a) Estimation of parvalbumin Ca^{2+}- and Mg^{2+}-binding constants by global least squares analysis of isothermal titration calorimetry data. *Anal. Biochem. 319,* 216-233.

36. Herzberg, O., and James, M.N. (1985). Structure of the calcium regulatory muscle protein Troponin-C at 2.8 Å resolution. *Nature 313,* 653-659.

37. Kozlov, A. G., and Lohman, T. M. (2000) Large contributions of coupled protonation equilibria to the observed enthalpy and heat capacity changes for ssDNA binding to *Escherichia coli* SSB protein. *Proteins 41,* 23—43.

38. Kretsinger, R.H. (1980) Structure and evolution of calcium-modulated proteins. *CRC Critical Rev. Biochem. 8(2):* 119-174.

39. Kretsinger, R.H., and Nockolds, C.E. (1973) Carp muscle calcium-binding protein. II. Structure determination and general description. *J. Biol. Chem. 248*, 3313-3326.

40. MacManus, J.P., Szabo, A.G., Williams, R.E. (1984) Conformational changes induced by binding of bivalent cations to oncomodulin, a paravalbumin-like tumor protein. Biochem J 1984; 220:261-268.]

41. MacManus, J.P., Whitfield, J.F. (1983) Oncomodulin: A calcium-binding protein from hepatoma. In: calcium and cell function. (Cheng, W.Y., Ed). Pp 411-440. Academic Press, New York.

42. MacManus, J.P., Whitfield, J.F., Boynton, A.L., Durkin, J.P., and Swierenga, S.H. (1982) Oncomodulin a widely distributed, tumor-specific, calcium-binding protein. *Oncodev. Biol. Med. 3(2-3),* 79-90.

43. McCrary, B. S., Bedell, J., Edmondson, S. P., and Shriver, J. W. (1998) Linkage of protonation and anion binding to the folding of Sac7d, *J. Mol. Biol. 276,* 203-224.

44. McCrary, B. S., Edmondson, S. P., and Shriver, J. W. (1996) Hyperthermophile protein folding thermodynamics: differential scanning calorimetry and chemical denaturation of Sac7d, *J. Mol. Biol. 264*, 784-805.

45. McPhalen, C.A., Sielecki, A.R., Santarsiew, B.D., and James, M.N. (1994) Refined crystal structure of rat parvalbumin a mammalian α-lineage parvalbumin, at 2.0 Å resolution. *J. Mol. Biol. 235(2),* 718-732.

46. McPhalen, C.A., Strynadka, N.C., and James, M.N. (1991) Calcium-binding sites in proteins: A structural perspective. *Adv. Protein Chem. 42*, 77–144

47. Moews, P. C., and Kretsinger, R. H. (1975) Terbium replacement of calcium in carp muscle parvalbumin: an X-ray crystallographic study. *J. Mol. Biol. 91*, 229-232.

48. Moncrief ND, Kretsinger RH, Goodman M. (1990) Evolution of EF-hand calcium-modulated proteins. I. Relationships based on amino acid sequences. *J Mol Evol. 30*, 522-562.

49. Monera, O.D., Shaw, G.S., Zhu, B.Y., Sykes, B.D., Kay, C.M., and Hodges, R.S. (1992) Role of interchain helical hydrophobic interactions in Ca^{2+} affinity, formation and stability of a two-site domain in troponin C. *Prot. Sci. 1*, 945-955.

50. Muntener, M., Kaser, L., Weber, J., and Berchtold, M.W. (1995). Increase of skeletal muscle relaxation speed by direct injection of parvalbumin cDNA. *Proc. Natl. Acad., Sci. USA. 92,* 6504-6508.

51. Mutus, B., Karuppiah, N., Sharma, R.K., and MacManus, J.P. (1985) The differential stimulation of brain and heart cyclic-AMP phosphodiesterase by oncomodulin. *Biochem. Biophys. Res. Commun. 13,* 500-506.

52. Nakayama, S., Moncrief, N.D., and Kretsinger, R. H. (1992) Evolution of EF-hand calcium-modulated proteins. II. Domains of several subfamilies have diverse evolutionary histories. *J. Mol. Evol. 34(5),* 416-448.

53. Novak, R., Brewer, J. M., and Ragland, W. L. (1996) Immunophenotype of splenic lymphocytes with receptors for avian thymic hormone. *FASEB J. 10,* A1048.

54. Novak, R., Henzl, M. T., and Ragland, W. L. (1997) Receptor cells for the CPV3 parvalbumin of chicken thymus in spleen and caecal tonsils. *J. Allergy Clin. Immunol. 99,* S202.

55. Ogawa, Y. (1985) Calcium binding to Troponin: effects of Mg^{2+}, ionic strength and pH. *J. Biochem. (97)4,* 1011- 1023.

56. Pack, A.K., and Slepecky, N.B. (1995) Cytoskeletal and calcium-binding proteins in the mammalian organ of Corti: cell type-specific proteins displaying longitudinal and radial gradients. *Hear. Res. 91,* 119-135.

57. Pauls, T.L., Durussel, I., Clark, I.D., Szabo, A.G., Berchtold, M.W., and Cox, J.A. (1996a) Site specific replacement of amino acid residues in the CD site of rat parvalbumin changes the metal specificity of this calcium/magnesium-mixed site toward a calcium/magnesium-mixed site toward a calcium-specific site. *Eur. J. Biochem. 242,* 249-255.

58. Pechere, J., Canopy, J.P., and Demaille, J.G. (1973) Evolutionary aspects of the structure of muscular parvalbumins. *Syst. Zool. 22,* 533-548.

59. Pechere, J., Canopy, J.P., Reyden, L., and Demaille, J.G. (1971) The amino acid sequence of the major parvalbumin from hake muscle. *Biochem. Biophys. Res. Commun. 43,* 1106-1111.

60. Sakaguchi, N., Henzl, M. T., Thalmann, I., Thalmann, R., and Schulte, B. A. (1998) Oncomodulin is Expressed Exclusively by Outer Hair Cells in the Organ of Corti. *J. Histochem. Cytochem. 46,* 29-39.

61. Schwaller, B., Dick, J., Dhoot, G., Carroll, S., Vrbova, G., Nicotera, P., Pette, D., Wyss, A., Buethmann, H., Hunziker, W., and Celio, M.R. (1999). Prolonged contraction-relaxation cycle of fast-twitch muscles in parvalbumin knockout mice. *Cell Physiol. 276(2),* C395-C403.

62. Senarita, M., Thalmann, I., Shibaski, O. and Thalmann, R. (1995) Calcium-binding proteins in the organ of Corti and basilar papilla: CBP-15, an unidentified calcium-binding protein of the inner ear. *Hear. Res. 90,* 169-175.

63. Simonides, W.S., and Van Hardeveld, C. (1989) The postnatal development of sarcoplasmic reticulum Ca^{2+} transport activity in skeletal muscle of the rat is critically dependent on thyroid hormone. *Endocrinology 124(3),* 1145-1153.

64. Strynadka, N.C., and James, M. N. (1989) Crystal structures of the helix-loop-helix calcium-binding proteins, *Ann. Rev. Biochem. 58,* 951-998.

65. Thalmann, I., Thalmann, R., and Henzl, M.T. (1998) Novel calcium sensor in the outer hair cells: quantitation of oncomodulin. *Prim. Sens. Neuron 2,* 283-296.

66. Yin, Y., Henzl. M. T., Lorber, B., Nakazawa, T., Thomas, T. T., Jiang, F., Langer, R., and Benowitz, L. I. (2006) Oncomodulin is a macrophage-derived signal for axon regeneration in retinal ganglion cells. *Nature Neurosci. 9,* 843-852.

67. Zheng, J., Shen, W., He, D.Z.Z., Long, K.B., Madison, L.D., and Dallos, P. (2000) Prestin is the motor protein of cochlear outer hair cells. *Nature 405,* 149-155.